Adsorption of Formamide at the Surface of Amorphous and Crystalline Ices under Interstellar and Tropospheric Conditions. A Grand Canonical Monte Carlo Simulation Study

Bálint Kiss[a,b], Sylvain Picaud[c], Milán Szőri[a], Pál Jedlovszky[d,*]

[a]*Institute of Chemistry, University of Miskolc, Egyetemváros A/2, H-3515 Miskolc, Hungary*

[b]*University of Lille, Faculty of Sciences and Technologies, LASIR (UMR CNRS 8516), 59655 Villeneuve d'Ascq, France*

[c]*Institut UTINAM (CNRS UMR 6213), Université Bourgogne Franche-Comté, 16 route de Gray, F-25030 Besançon, France*

[d]*Department of Chemistry, Eszterházy Károly University, Leányka u. 6, H-3300 Eger, Hungary*

*E-mail: jedlovszky.pal@uni-eszterhazy.hu

Abstract:

The adsorption of formamide is studied both at the surface of crystalline (I_h) ice at 200 K and at the surface of low density amorphous (LDA) ice in the temperature range of 50-200 K by grand canonical Monte Carlo (GCMC) simulation. These systems are characteristic to the upper troposphere and to the interstellar medium (ISM), respectively. Our results reveal that, while no considerable amount of formamide is dissolved in the bulk ice phase in any case, the adsorption of formamide at the ice surface under these conditions is a very strongly preferred process, which has to be taken into account when studying the chemical reactivity in these environments. The adsorption is found to lead to the formation of multimolecular adsorption layer, the occurrence of which somewhat precedes the saturation of the first molecular layer. Due to the strong lateral interaction acting between the adsorbed formamide molecules, the adsorption isotherm does not follow the Langmuir shape. Adsorption is found to be slightly stronger on LDA than I_h ice under identical thermodynamic conditions, due to the larger surface area exposed to the adsorption. Indeed, the monomolecular adsorption capacity of the LDA and I_h ice surfaces is found to be 10.5 ± 0.7 μmol/m^2 and 9.4 μmol/m^2, respectively. The first layer formamide molecules are very strongly bound to the ice surface, forming typically four hydrogen bonds with each other and the surface water molecules. The heat of adsorption at infinitely low surface coverage is found to be -105.6 kJ/mol on I_h ice at 200 K.

1. Introduction

Formamide, the smallest molecule containing a peptide bond, is present in abundance both on Earth, including its atmosphere, and also in the space. Thus, amides are emitted directly to the Earth atmosphere from biological sources as well as from industrial processes (e.g. formamide can serve as a solvent, plasticizer, or as a substance associated with a blowing agent used in the creation of foam).[1] Large amount of amides can also form directly in the atmosphere *via* oxidation of amines available. In particular, methylamine, the smallest alkyl amine, the oxidation of which can lead to formamide, has a global emission of 24 ± 15 Gg N yr^{-1}.[2] Atmospheric level of amides is in the range of pptv, and they have been detected in ambient particles, biomass burning aerosols and fogwater, as well.[3-5] Carbon capture and storage (CCS) technology may represent a significant source of amides to ambient air in the future, since formamide was detected from an industrial scale carbon capture.[6] However, up to now only a few investigations have been carried out to understand the atmospheric fate of amides.[7] Photolysis can be a negligible sink for amides, as indicated by a study of cross-section measurement.[8] On the other hand, oxidation can be a relevant process concerning the atmospheric loss of formamide. Barnes *et al.* determined rate coefficients for the reaction of OH·, Cl, NO_3 and O_3 with formamide at room temperature by means of *in situ* FTIR spectrometry.[9] The established rate constant of the formamide + OH· reaction was also confirmed using proton transfer reaction−mass spectrometry (PTR-MS) detection by two independent research groups.[7,10] The corresponding atmospheric lifetime of formamide was estimated to be a few days.[9] Due to the high affinity of formamide to water, uptake and subsequent deposition is proposed to be as another important sink,[11,12] although, to the best of our knowledge, it was never investigated. In the troposphere, such an uptake might predominantly involve adsorption at the surface of ice grains.

Further, besides its presence in the atmosphere of the present day Earth, formamide is generally thought to be present at Earth also in the prebiotic time. Indeed, an increasing body of both experimental[13-15] and theoretical[16-18] evidences point to formamide as a possible hub in the complex network of prebiotic chemical reactions leading from simple precursors, such as H_2, H_2O, N_2, NH_3, CO, and CO_2, to key biological molecules. The one-pot formamide-based chemistry affords the synthesis of nucleobases (i.e., adenine, guanine, uracil, and isocytosine)

without isolation and/or purification of specific intermediates, along with a variety of organic compounds including carbohydrates, amino acids and carboxylic acids with reasonably good yield.[19] The 'HCN World' hypothesis[20,21] is also strongly related to prebiotic formamide chemistry,[22,23] since the hydrolysis of HCN to formamide prevails over HCN polymerization at low enough (i.e., below 0.01mol/dm^3) HCN concentrations.[24] High enough (above 1 mol/dm^3) HCN concentrations, needed to promote the polymerization route towards nucleobases, only plausibly occurred locally, at interfaces. Indeed, a previous molecular dynamics simulation showed interfacial abundance and lateral self-association of HCN molecules, exhibiting also enhanced dynamical stability at the surface of their aqueous solutions.[25] Lateral self-association of the adsorbed HCN molecules was also shown to be present at the surface of ice.[26] These floating HCN patches might well provide spots for HCN polymerization.[25] Although these simulation studies support the freeze-concentration model,[27] the competition between HCN polymerization and hydrolysis to formamide still has to be considered.[28,29]

Formamide has also been detected in galactic centers,[30,31] star-forming regions of dense molecular clouds,[32] high-mass young stellar objects,[33] the interstellar medium,[34] comets,[35-37] and satellites.[38] Although its formation, whether on the surfaces of the interstellar grains or in the gas phase, is currently under debate, recent quantum chemical calculation of two competitive reaction channels (i.e., $NH_2 + \cdot HCO$ and $\cdot CN + H_2O$) suggested plausible formamide formation routes in presence of amorphous ice (mimicked by 33 water molecules).[39] Since the temperature of the interstellar medium (ISM) is supposed to be below 110 K, eutectic aqueous mixture of formamide cannot play important role at the interstellar conditions (as the eutectic temperature, corresponding to 60 mol% formamide, is 227.85 K).[40] High energy particles (e.g., cosmic ray, solar wind), heat, electromagnetic radiation, and radioactive decay continuously interact with simple chemical precursors, such as formamide, to yield new complex derivatives. If the activated molecule can interact with the proper reactant, then amino acids, nucleobases, sugars, lipids, and carboxylic acids can emerge as very easily synthesizable molecules.[41] However, under the extremely low densities present in the ISM, sufficient formamide chemistry requires strong local enhancement of the formamide concentration. Such sites of locally high formamide concentration can again be expected at the surfaces of icy objects, such as cometary[42] or interstellar[43] dust grains that are frequently covered by low density amorphous ice (LDA). Finally, it is important to note that if formamide

is formed on solid surfaces, its gas-phase detection and the subsequent (photo)chemistry processes would thus strongly depend on the formamide interaction with water molecules.[44,45]

Thus, while a detailed understanding of the adsorption of formamide at the surface of crystalline (I_h) ice at tropospheric temperatures (i.e., around 200 K) is important from the point of view of atmospheric chemistry, its adsorption on amorphous ice (LDA) under interstellar conditions, i.e., at temperatures below 110 K, is a process of relevance in astrochemistry, with a special importance also in the field of prebiotic evolution. However, due to the extreme conditions, experimental investigation of these problems is far from being straightforward. Computer simulation methods,[46] on the other hand, offer a very powerful tool to complement experimental investigations, as they can provide a full, three-dimensional insight into the structure of a suitably chosen model of the system of interest in atomistic resolution. In particular, adsorption processes can easily be studied in detail by grand canonical Monte Carlo (GCMC) simulation,[46,47] in which the chemical potential rather than the number of adsorbate molecules is controlled. Thus, by systematically varying the chemical potential and determining the number of adsorbed molecules as its function, the adsorption isotherm can easily be calculated. Indeed, the GCMC method has successfully been used to simulate the adsorption of various small molecules at the surface of, among others, clay minerals (e.g., kaolinite),[48,49] zeolites,[50-56] various metal oxides,[57-60] crystalline[26,61-69] as well as amorphous ice,[70] various carbonaceous materials,[71-77] self-assembled aerosol monolayers,[78,79] and covalent organic frameworks,[80-82] as well as inside protein crystals[83] and clathrate cages.[84-91]

In this paper, we investigate in detail the adsorption of formamide both at the surface of I_h ice (at 200 K) and at the surface of LDA ice (at 200 K, 100 K, and 50 K). Although the adsorption on LDA at 200 K has relevance neither in atmospheric chemistry nor in astrochemistry, we included this system in the present investigation for reference purposes. Namely, this way the dependence of the adsorption both on the phase of the adsorbent (i.e., crystalline vs. amorphous) and on the temperature (for LDA ice) can also be addressed. The results are discussed in terms of the adsorption isotherms, density profile of the adsorption layer, as well as binding energy and surface orientation of the adsorbed molecules that belong to the first molecular layer (i.e., that are in direct contact with the ice phase). This information can provide interesting support for the interpretation of experimental and observational data. Indeed, thermal desorption experiments[45,92] as well as simplified chemical models[44] indicate that the binding energy of formamide on water ice is larger than the interaction between water

ice molecules, which is easily checkable in our GCMC simulations. In addition, the detailed analysis of the molecular orientations in the simulations can give important information on the orientation and surrounding of the C=O bond, which corresponds to an intense spectral feature usually easily identifiable in infrared observations.[92]

The paper is organized as follows. In section 2, details of the calculations performed, including the GCMC simulations and the identification of the first layer adsorbed molecules are given. The obtained results are discussed in detail in section 3, while in section 4 the conclusions of this study are summarized.

2. Methods

2.1. Grand Canonical Monte Carlo Simulations. The adsorption of formamide at the surface of both crystalline (I_h) and amorphous (LDA) ice has been simulated on the grand canonical (μ,V,T) ensemble by the GCMC[46,47] method. Simulations involving amorphous ice have been performed at the temperatures of 50 K, 100 K, and 200 K, while adsorption on I_h ice has only been simulated at 200 K. The number of the water molecules in the basic box has been fixed to 2880 in every simulation. To obtain the adsorption isotherms, with each adsorbent and every temperature a set of GCMC simulations have been performed, in which the chemical potential, μ, of formamide has been systematically varied from values corresponding to practically no formamide molecule to those at which formamide fills the available space in the basic box. The number of the adsorbed formamide molecules has then been determined as a function of the chemical potential. The formamide chemical potential values considered in the different systems are collected in Tables 1-4. The X, Y, and Z edges of the rectangular basic simulation box have been 100 Å, 35.926 Å, and 38.891 Å, respectively, axis X being perpendicular to the macroscopic plane of the ice surface.

Water and formamide molecules have been described by the three-site SPC/E potential[93] and by the CHARMM27 force field,[94] respectively, since this model combination was previously found to best reproduce the mixing properties of water and formamide.[95] In both of these potential models, interactions are centered at the individual atoms. Thus, the interaction energy of a molecule pair is calculated as the sum of the Lennard-Jones and charge-charge Coulomb contributions of their individual atom pairs, while the total energy of the

system is calculated as the sum of the interaction energies of all molecule pairs. In the simulations, all molecules have been treated as rigid bodies, and all interactions have been truncated to zero beyond the center-center cut-off distance of 12.5 Å.

The simulations have been performed using the program MMC.[96] In every Monte Carlo step either a randomly chosen molecule has been randomly translated by no more than 0.25 Å and randomly rotated around a randomly chosen space-fixed axis by no more than 15°, or a formamide molecule has been tried to be either inserted to, or deleted from the system. Particle displacement and insertion/deletion attempts as well as formamide insertion and deletion attempts have been done with equal probabilities. Insertion and deletion attempts have been done according to the cavity biased scheme of Mezei,[97,98] thus, insertions have only been attempted into pre-existing empty cavities of the radius of at least 2.5 Å. Such cavities have been searched for in the basic box along a 100×100×100 grid, regenerated after every 10^6 Monte Carlo steps. Insertion and deletion attempts have been accepted or rejected according to the cavity biased scheme.[97,98] The probability of finding a suitable cavity, P_{cav}, occurring in these acceptance criteria, has simply been estimated as the ratio of the number of suitable cavities found and grid points tested in configurations consisting of exactly N formamide molecules.[97,98] Acceptance of the particle displacement trials have been decided according to the standard Metropolis criterion.[46,99] The fraction of the successful particle displacement and insertion/deletion trials have turned out to be about 5% and 0.0001%, respectively, at the lowest temperatures.

In preparing the I_h phase of ice, the water molecules have been arranged in 18 layers, consisting of 160 molecules each, along the interface normal axis, X, in such a way that the two surfaces correspond to the (0001) surface of I_h ice. The LDA phase has been created by thermalizing the I_h phase at 300 K in a 10^8 Monte Carlo steps long run, followed by a 2×10^8 Monte Carlo steps long run at 350 K, and another 10^8 Monte Carlo steps long run again at 300 K. Finally, the system has been quenched to 200 K, and equilibrated for 10^8 Monte Carlo steps at this temperature. At the beginning of each simulation, two formamide molecules have been placed in the basic box far from the ice phase. The systems have been equilibrated for 1.5×10^9 - 2×10^{10} Monte Carlo steps, until both the number of the formamide molecules present in the basic box and the total energy of the system stopped showing even traces of a tendentious change. The need for such an unusually long equilibration period came from the unusually small acceptance rate of the trial moves, in particular, that of the insertion/deletion

attempts, at low temperatures. The number of the formamide molecules present in the basic box has then been averaged over a subsequent, 10^9 Monte Carlo steps long equilibrium run. Finally, at selected chemical potential values, indicated also in Tables 1-4, 5000 equilibrium sample configurations per system, separated from each other by 5×10^5 Monte Carlo steps, have been dumped for detailed analyses from 2.5×10^9 Monte Carlo steps long production runs. Equilibrium snapshots of the 50 K system, simulated at these four selected chemical potential values, covering the adsorption range from only a few adsorbed formamide molecules to multilayer adsorption, are shown in Figure 1.

2.2. Identification of the First Layer Adsorbed Molecules. Since the surface of the amorphous ice phase, unlike that of crystalline ice, is corrugated, on the molecular length scale, by capillary waves, the adsorbed formamide molecules that belong to the first molecular layer (i.e., that are in direct contact with the amorphous ice phase) cannot be identified as simply as in the case of crystalline ice. Thus, while in the latter case the first adsorbed molecular layer is conventionally defined through the first minimum of the adsorbate density profile,[26,61-69] at the surface of amorphous ice these molecules have to be identified by means of an appropriate intrinsic surface analyzing method. Several such methods have been proposed in the past 15 years,[100-106] among which the Identification of the Truly Interfacial Molecules (ITIM)[103] turned out to be an excellent compromise between accuracy and computational cost.[104] Therefore, here we have identified the first layer formamide molecules adsorbed at the surface of amorphous ice using the ITIM method.

In an ITIM analysis, probe spheres of a given radius are moved towards the phase of interest from the bulk opposite phase (in our case, towards the adsorption layer from the middle of the ice phase) along test lines perpendicular to the macroscopic plane of the interface. Formamide molecules that are first touched by the moving probe along any test line (i.e., that are "seen" by the probe from the ice phase) are then considered as belonging to the first molecular layer, while formamides that are never touched by the probe belong to one of the subsequent layers. In accordance with earlier findings concerning the optimal performance of the ITIM method for systems of small molecules,[103,104] here we used a probe sphere of the radius of 1.5 Å and a grid spacing of 0.4 Å along both the *Y* and *Z* axes. In deciding whether a formamide molecule is touched by the probe, its atoms have been represented by spheres with the diameter equal to the corresponding Lennard-Jones distance parameter, σ. Since practically

no formamide molecules have been found either to be dissolved in the bulk ice phase, or in the vapor phase, to be isolated from the adsorption layer in any case, no modification of the original ITIM algorithm had to be made. The first layer formamide molecules identified this way are also indicated in Fig. 1.

3. Results and Discussion

3.1. Adsorption Isotherms and Density Profiles. *3.1.1. Adsorption Isotherms.* The adsorption isotherms obtained from the simulations are shown in Figure 2 in the form of number of adsorbed formamide molecules as a function of their chemical potential. Since negligible fraction of the formamide molecules are either dissolved in the bulk ice phase or stay isolated from the adsorption layer in the vapor phase in every case, we simply took the total number of formamide molecules in the basic box as the number of the adsorbed molecules. As is seen, the isotherm obtained on I_h ice rises continuously up to the chemical potential value of about -60 kJ/mol. This rising part is followed by a plateau in the μ range of about -60 – -57 kJ/mol, corresponding to an adsorption monolayer. This monolayer is rather stable, as evidenced by the fact that it exists in an about 3 kJ/mol wide range of chemical potentials. The plateau is followed by a very steeply rising part of the isotherm, corresponding to multilayer adsorption. This steeply rising part of the isotherm ends at the chemical potential value of about -57 kJ/mol, where the basic box becomes filled with formamide molecules.

The isotherm obtained at 200 K on LDA ice is very similar to that corresponding to crystalline ice, with two notable differences. First, the plateau observed between -60 and -56 kJ/mol on I_h ice is missing on LDA ice, instead, the isotherm rises continuously even in this μ range, exceeding the isotherm corresponding to I_h ice. This finding suggests that the corrugated geometry of the LDA surface, resulting also in corrugations of the first adsorption layer, promotes multilayer adsorption. As a consequence, multilayer adsorption on LDA starts at μ values at which the adsorbed monolayer is still stable on I_h ice. Second, the basic box can host considerably more formamide molecules in the presence of LDA than I_h ice. This difference simply reflects that the density of LDA ice is higher than that of I_h ice. The shape of the $<N>(\mu)$ isotherm does not change noticeably with the temperature, it is simply shifted to higher chemical potential values as the temperature decreases.

An important feature of the obtained isotherms is that they also have a point on their very sharply rising part, preceding immediately the filling of the basic box, in most of the cases. Usually this very sharp rise of the isotherm is interpreted as the condensation of the adsorbate. Our present finding indicates, however, that condensation is preceded by the occurrence of a thick, multimolecular adsorption layer. Therefore, the possibility that the thickness of the adsorption layer of formamide can be comparable with the width of the slab between the two ice surfaces in the basic box (being about 30 Å), or might even well exceed it, cannot be excluded. If this is indeed the case, the filling of the basic box simply indicates the point at which the adsorption layer gets as thick as this slab rather than the point of condensation of formamide. To check this possibility, and determine the real point of condensation without the above finite size effect error, we have performed a set of GCMC simulations of neat formamide (i.e., in the absence of the ice phase) in the same basic box at each of the three temperatures considered. Since the point of condensation is a value characteristic to the adsorbate itself, being independent from the type and even from the presence or absence of any adsorbent, its value can unambiguously be determined in the lack of the ice phase. Indeed, we observed a very sharp transition from a practically empty to a filled basic box at a given chemical potential value at every temperature considered. Thus, the chemical potential value corresponding to the point of condensation, μ_0, has turned out to be -41.521 kJ/mol at 200 K, -22.947 kJ/mol at 100 K, and -11.432 kJ/mol at 50 K, indeed well above the μ values corresponding to the sharply rising part of the isotherms. The temperature dependence of the obtained μ_0 values is shown in the inset of Fig. 2. As is seen, the $\mu_0(T)$ points are laying along a straight line. Considering the fact that, for a one component system, the chemical potential is equivalent with the molar free energy, and hence, apart from a minus sign, its temperature derivative with the molar entropy, S^m (i.e., $S^m = -(\partial\mu/\partial T)$), our result suggests that the molar entropy of formamide is constant (i.e., temperature independent) at the point of condensation, being 198.5 ± 11.0 J/mol K.

In order to further analyze the adsorption isotherms, we have converted them to the more conventional Γ vs. p_{rel} form, where Γ is the surface density of formamide, calculated as

$$\Gamma = \frac{< N >}{2YZ}, \qquad (1)$$

In this equation, the factor 2 in the denominator reflects the presence of two ice surfaces in the basic box. Further, p_{rel} is the relative pressure of the vapor phase (i.e., its pressure, p, normalized by that of the saturated vapor, p_0). The value of p_{rel} can be calculated from that of μ, using also the chemical potential value corresponding to the point of condensation, μ_0, as[59]

$$p_{rel} = \frac{p}{p_0} = \frac{\exp(\mu / k_B T)}{\exp(\mu_0 / k_B T)}, \tag{2}$$

where k_B stands for the Boltzmann factor. It should be noted that in converting the $<N>(\mu)$ isotherms to the $\Gamma(p_{rel})$ form, we have omitted the points corresponding to filled basic box (as they are affected by finite size effect error).

The obtained $\Gamma(p_{rel})$ isotherms are shown in Figure 3. As is seen, at 200 K, the isotherms start rising almost linearly, this rise gradually decreases turning into a plateau, and the plateau part is followed by a second, steeply rising part of the isotherms. The first rising part corresponds to the gradual building up of the first molecular layer; the plateau reflects the presence of a more or less saturated monolayer, while the second, steeply rising part corresponds to multilayer adsorption. At lower temperatures, the plateau of the isotherm gets progressively shorter and occurs at lower surface densities, suggesting that multilayer adsorption starts before the complete saturation of the first molecular layer. Thus, the obtained isotherms represent a transition between type II and type III isotherms (both describing multilayer adsorption) according to the IUPAC convention. Considering that type II isotherms correspond to systems where the adsorbate-adsorbent interaction is considerably stronger, while type III isotherms correspond to systems where it is considerably weaker than the lateral interaction between the adsorbed molecules, this result is in a clear accordance with earlier claims that the mixing of water and formamide is nearly ideal,[95,107,108] and hence there is no marked difference between the interactions of the like and unlike molecules. Furthermore, it is also seen that the steepness of the first rising part of the isotherm, corresponding to the building up of the first molecular layer, increases very strongly with decreasing temperature, which results in a very sharp rise of the low temperature isotherms even at extremely low p_{rel} values.

We tried to fit the $\Gamma(p_{rel})$ data up to their plateau region by the Langmuir isotherm,[109,110] i.e.,

$$\Gamma = \Gamma_{\max} \frac{p_{\mathrm{rel}} K}{1 + p_{\mathrm{rel}} K}, \tag{3}$$

where the parameters $\Gamma_{\max}$ and K are the surface density of the saturated monolayer and the Langmuir partition coefficient, measuring the partitioning of the adsorbate molecules between the adsorption layer and the vapor phase, respectively. However, we could not get a reasonable fit in any case (see Fig. 3), suggesting that there might well be strong lateral interaction between the adsorbed formamide molecules. This point will be investigated in detail in a subsequent part of this paper. Nevertheless, the Langmuir function can still be fitted to the nearly linearly rising, very low p_{rel} points (i.e., the ones corresponding to considerably smaller Γ values than that corresponding to the plateau region) in the simulated data sets. Although the $\Gamma_{\max}$ values resulting from these fits are meaningless, as they are affected by far too large numerical error, the K values can still serve at least as rough estimates of the formamide partitioning between the adsorption layer and the vapor phase. This way, the value of K has turned out to be about 5×10^4 at 200 K, 6×10^{18} at 100 K, and 10^{43} at 50 K. Although these values are still affected by large error bars, their very high orders of magnitude indicate strongly increasing affinity of formamide to the LDA surface with decreasing temperatures.

Based on the behavior of the obtained isotherms, we have selected four chemical potential values in each system, at which sample configurations have been collected for detailed analyses. The lowest of these chemical potential (referred to here as state I) always corresponds to only a few adsorbed molecules per surface. At the second μ value chosen (state II), formamide molecules form an unsaturated monolayer, but cannot be isolated from each other, while the third μ value (state III) they form a more or less saturated monolayer. Finally, the largest of the chosen chemical potential values (state IV) corresponds to multilayer adsorption (i.e., when the basic box is already filled with formamide molecules) in every case. The chemical potential values corresponding to these states are indicated in Tables I-IV as well as in Fig. 2.

3.1.2. Density Profiles. The mass density profiles of all formamide molecules as well as only those forming the first molecular layer at the ice surface along the surface normal axis, X, are shown in Figure 4, as calculated in states I-IV in the various systems considered. The obtained profiles clearly confirm our earlier claim that no substantial amount of formamide is

located in the vapor and in the bulk ice phase. For reference, the mass density profile corresponding to the outmost portion of the ice phase is also indicated, while the inset of the figure shows the comparison of the density profiles of the I_h and LDA ice phases at 200 K. As is seen, while the density profile of I_h ice shows the clear separation of the subsequent molecular layers in the ice crystal, that of LDA is practically constant inside the bulk phase. It is also seen that the ordered structure of I_h ice implies also a clear layering of the adsorbed formamide molecules in the case of multilayer adsorption, while this layering is effectively screened by the corrugated surface of LDA ice.

The comparison of the profiles corresponding to all formamide molecules and to only those belonging to the first molecular layer reveals that not even traces of multilayer adsorption occur in states I-III. Further, since the saturated adsorption monolayer can be very well estimated by the first molecular layer in state IV, it is also evident that the adsorption monolayer in state III is clearly not yet saturated in any case (see also Fig. 1). Since state III has always been chosen as the point immediately preceding the sharp rise of the isotherm, this finding is in a clear accordance with our earlier claim that multilayer adsorption starts before the first monolayer gets saturated.

Integration of the density profiles of the first layer formamide molecules in state IV provides the average number of first layer adsorbed molecules, and hence also the surface density of the saturated monolayer, Γ_{max}. Assuming that the surface area of the LDA phase is independent from the temperature, the value of Γ_{max} turns out to be 10.5 ± 0.7 μmol/m^2 for LDA, and 9.4 μmol/m^2 for I_h ice. The fact that the value of Γ_{max} is significantly larger for LDA than for I_h ice reflects that considerably more adsorbed molecules can be accommodated at the corrugated surface of amorphous ice than at the flat surface of crystalline ice. Similar results were obtained earlier concerning the adsorption of methylamine at LDA and I_h ice surfaces.[70] Further, the fact that the obtained Γ_{max} values are considerably larger than the surface densities corresponding to the plateau region of the $\Gamma(p_{rel})$ isotherms, scattering between about 6 and 8 μmol/m^2 (see Fig. 3) stresses again that multilayer adsorption precedes the saturation of the first molecular layer at formamide at the surface of both amorphous and crystalline ice.

Finally, having the Γ_{max} values estimated, we can attempt to establish a relation between the calculated isotherms and the possible adsorption of formamide on LDA under interstellar, and on I_h ice under tropospheric conditions. For this, the p_0 values corresponding to

the temperatures considered are needed to be, at least, estimated. Such estimation can be given by the Antoine equation:[111]

$$\ln p_0 = A - \frac{B}{T + C}, \tag{4}$$

where *A*, *B*, and *C* are the Antoine parameters. Unfortunately, the only Antoine parameter set for formamide we are aware of, i. e., $A = 5.9526$, $B = 8937.035$ K, and $C = 27.655$ K, corresponding to the p_0 value in Pa units, is supposed to provide reliable results only in the temperature range between 343.7 K and 483.7 K,[112,113] well above the temperature range of our interest. Nevertheless, using the p_0 value corresponding to the lower boundary of this range of 343.7 K as a very crude but certainly upper estimate of the p_0 value at the temperatures considered in this study, and converting the pressure values to bulk vapor phase concentration using the ideal gas law, the vapor phase concentration of formamide being in equilibrium with the saturated adsorption monolayer (i.e., Γ being 10.5 μmol/m^2 for LDA and 9.4 μmol/m^2 for I_h ice) can be estimated as 10^{-17} molecules/dm^3 at 50 K, 10^5 molecules/dm^3 at 100 K, and 10^{15} molecules/dm^3 at 200 K. Considering that the concentration of formamide is thought to be about $10^{-1} – 10^{-2}$ molecules/dm^3 at least in some parts of the ISM,[32] we can clearly conclude that its adsorption at the LDA surface is strongly preferred at 50 K. Further, given the crudeness of the estimation of p_0 we could make, being several orders of magnitude too high at the temperatures considered here, it is also quite possible that this preference of formamide for adsorption still prevails up to 100 K under interstellar conditions. Further, since the concentration of formamide in the atmosphere is thought to be about 2.5×10^{13} molecules/dm^3,[114] and taking into account again that our above estimate of 10^{15} molecules/dm^3 is very probably deviating several orders of magnitude up from the real value, our results strongly suggest that the adsorption of formamide on I_h ice under tropospheric conditions is also a strongly preferred process.

3.2. Orientation of the First Layer Formamide Molecules. Since the orientation of a rigid molecule relative to an external direction (or plane) can be described by two independent orientational variables, their orientational statistics can only be fully characterized by the bivariate joint distribution of these two variables.[115,116] We showed previously that the angular polar coordinates ϑ and ϕ of the external vector (in our case, the macroscopic surface normal

vector, $\underline{X}$, pointing, by out convention, away from the ice phase) in a local Cartesian frame fixed to the individual molecules is a suitable choice for such a pair of independent orientational variables.[115,116] Here we define this local Cartesian frame in the following way. Its origin coincides with the N atom of the formamide molecule, axis *x* points along the N-C bond from the N to the C atom, axis *z* is perpendicular to the plane of the molecule, while axis *y* is perpendicular to both axes *x* and *z*, and it is oriented in such a way that the *y* coordinate of the O atom is positive. Thus, the polar angle ϑ is the angle between the macroscopic surface normal axis, *X* (i.e., edge *X* of the basic box) and the molecule normal, while angle ϕ is the angle between the projection of $\underline{X}$ to the molecular plane and the vector pointing from the N to the C atom of the formamide molecule. The definition of this local Cartesian frame as well as that of the polar angles ϑ and ϕ is illustrated in Figure 5a. It should be noted that, due to the planar symmetry of the formamide molecule, this local frame can always be chosen in such a way that the polar angle ϑ does not exceed 90°, and thus $0 \leq \cos\vartheta \leq 1$. Finally, since ϑ is an angle formed by two general spatial vectors, but ϕ is formed by two vectors that stay, by definition, within a given plane (i.e., the molecular plane), uncorrelated orientation of the molecules with the surface results in a uniform distribution only if $\cos\vartheta$ and ϕ are chosen to be the orientational variables.[116]

The $P(\cos\vartheta,\phi)$ orientational maps of the first layer formamide molecules are shown in Figure 6 as obtained from our simulations. As is seen, there are two preferred orientations of these molecules. The first one, occurring at the $\cos\vartheta$ value of 1, corresponds to the parallel alignment of the molecule with the macroscopic plane of the ice surface (i.e., the *YZ* plane of the basic box). This orientation is denoted here as I_{FA}. (It should be noted that in the case of $\cos\vartheta = 1$, the projection of $\underline{X}$ to the *xy* plane of the local frame becomes a single point, see Fig. 5a, thus angle ϕ loses its meaning, and hence all points of the $P(\cos\vartheta,\phi)$ orientational map laying along the $\cos\vartheta = 1$ line are equivalent.) The peak corresponding to the second preferred orientation, marked here as II_{FA}, is located at ϕ values close to 360°, and it extends largely along the $\cos\vartheta$ axis of the map. This peak corresponds to a tilted orientation of the formamide molecule in such a way that the molecular plane is not twisted substantially with respect to the surface plane, and the NH_2 group points toward, while the CHO group away from the ice phase. Since the tilt angle in this alignment is right the polar angle ϑ, the extension of the II_{FA} peak along the $\cos\vartheta$ axis of the map indicates that various, differently tilted alignments of the

formamide molecule are all preferred. The preferred alignments I_{FA} and II_{FA} of the formamide molecules are illustrated in Figure 5b. Similar orientational preferences were obtained earlier at the liquid-vapor interface of water-formamide mixtures.[117]

The preference of the formamide molecules for these orientations can be understood by considering the possible hydrogen bonds they can form with each other as well as with the surface water molecules in these alignments. Since all the H-bonding directions of the formamide molecule lay also within the molecular plane, formamide molecules of alignment I_{FA} can easily hydrogen bond to each other; a formamide molecule of orientation I_{FA} can form up to four such H-bonds with its formamide neighbors. Further, since the surface of LDA ice is corrugated on the molecular length scale, two neighboring surface formamide molecules of alignment II_{FA}, located at different depths along the macroscopic surface normal axis, *X*, can also form a H-bond with each other in such a way that the molecule being farther from the bulk ice phase along this external axis is the H-donor, while the one being closer to the bulk ice phase is the H-acceptor partner. These possible hydrogen bonds between two surface formamide molecules, both aligned in one of their preferred orientations, are illustrated in Figure 5c.

Water molecules prefer four distinct orientations at the surface of I_h ice, in each of which one H-bonding direction (i.e., an O-H bond or a lone pair) is staying perpendicular to the surface plane.[70] At the surface of LDA ice, these preferences are much less sharp, the corresponding peaks of the orientational map are strongly merged, indicating that surface waters can rather largely deviate from these orientations. As a consequence, the co-planar alignment with the macroscopic plane of the surface is also preferred here.[70] A formamide molecule of orientation I_{FA}, laying also parallel with this plane, can thus easily form up to 4 H-bonds also with surface waters of this alignment. Moreover, even at the surface of I_h ice, a slight deviation from the alignment I_{FA} as well as from a preferred water orientation and/or a slight distortion of the linearity of the H-bond can also lead to the formation of several H-bonds between surface waters and I_{FA} aligned formamides. Furthermore, a formamide molecule of alignment II_{FA}, being tilted from the surface plane, can easily donate both of its NH_2 hydrogen atoms to surface water molecules aligned in two of their preferred orientations. These possible H-bonding patterns between surface water and first layer formamide molecules are also illustrated in Fig. 5c. The possible hydrogen bonding of the first layer formamide molecules is further investigated in the subsequent sub-section.

3.3. Energetics of the Adsorption. To characterize the energetic background of the adsorption, we have calculated the U_b binding energy (i.e., the total interaction energy with the rest of the system) of the first layer formamide molecules. Further, besides U_b, its contributions coming from the interaction with the ice phase, and with the other formamide molecules, denoted here as U_b^{ice} and U_b^{lat}, respectively, have also been calculated. The binding energy distributions obtained at 200 K, 100 K, and 50 K are shown in panels a, b, and c, respectively, of Figure 7.

The distributions obtained on I_h and LDA ices (Fig. 7a) are rather similar to each other, with the only notable difference that they are somewhat broader in the case of amorphous than crystalline ice, and this broadening is such that the $P(U_b^{ice})$ distributions extend to lower, while the $P(U_b^{lat})$ ones to higher energies in the case of LDA ice. This increased importance of the formamide-water interaction at the surface of amorphous ice can be well explained by the higher orientational flexibility of the water molecules as well as the by the larger amount of accessible H-bond donor and acceptor water partners at this surface than at that of I_h ice.[70] The opposite effects of the ice phase on the $P(U_b^{ice})$ and $P(U_b^{lat})$ distributions largely cancel each other, resulting in almost identical $P(U_b)$ distributions at the surface of the two ice phases, indicating again that the exchange of the H-bonded water and formamide neighbors of a formamide molecule has a negligible energetic consequence.

In state I, the $P(U_b^{ice})$ distribution of the 200 K systems exhibits a single peak around -100 kJ/mol. With increasing chemical potential (i.e., increasing surface coverage), this peak shifts to higher energies, often being splitted to two distinct peaks or, at least, exhibiting a shoulder. These peaks and shoulders typically occur around the energy values of about -75 kJ/mol, -50 kJ/mol, and -25 kJ/mol; in the case of state IV and I_h ice even a small peak of $P(U_b^{ice})$ around zero energy is seen. Considering that the energy of a hydrogen bond is roughly -25 kJ/mol, this finding indicates that in state I (i.e., at the lowest surface density considered), first layer formamide molecules typically form four H-bonds with the ice phase, and the number of their H-bonded water neighbors gradually decreases with increasing surface density.

On the other hand, the $P(U_b^{lat})$ distribution exhibits a very high and narrow peak at zero energy in state I; this peak is still clearly seen in state II and traces of it exist even in state III. This peak corresponds to the adsorbed formamide molecules that are isolated from each other. Interestingly, this distribution also shows a peak at around -25 kJ/mol even in state I on LDA ice, indicating that adsorbed molecules are not completely isolated from each other even in this state of very low surface density (i.e., when less than 5 formamides are attached, on average, to each of the two ice surfaces in the basic box, see Table 3). This behavior is in a clear contrast with our previous observation concerning the adsorption of methylamine on LDA ice,[70] and stresses the strong lateral interaction between the adsorbed formamide molecules. It should be noted that, by contrast with the LDA ice, no such peak is seen on $P(U_b^{lat})$ in state I of I_h ice, indicating that in this case the adsorbed molecules are indeed isolated from each other. The increase of the chemical potential, and hence that of the surface density shifts the $P(U_b^{lat})$ distribution to lower energies, reflecting the fact that adsorbed molecules are increasingly surrounded by each other. Thus, in LDA ice, the peak of the distribution occurs around -25 kJ/mol, -55 kJ/mol, and -80 kJ/mol in states II, III, and IV, respectively, indicating the ability of the adsorbed formamide molecules to form up to three H-bonds with each other.

The distribution of the total binding energy, $P(U_b)$, exhibits a single peak around -100 kJ/mol in states I-III, reflecting the compensation of the decrease of its ice, and increase of its lateral component (in magnitude) with increasing chemical potential, and indicating that adsorbed formamide molecules always prefer to form four hydrogen bonds with their neighbors, irrespectively of whether they are waters or formamides. Interestingly, in state IV the $P(U_b)$ peak occurs around -120 kJ/mol. Since a formamide molecule cannot form more than 4 hydrogen bonds, this deep binding energy reflects also the strong but non-hydrogen bonding interaction of the first layer formamide molecules with those forming the subsequent, outer molecular layers of the adsorption layer. Considering that first layer formamides already complete their four possible H-bonds with surface waters and in-layer formamides in the lack of outer adsorbed molecular layers, as seen from the $P(U_b)$ distributions in states I-III, we can conclude that their interaction with the subsequent layers in state IV most likely involves

strong dipolar interactions, as without that the additional, roughly -20 kJ/mol of the binding energy could not be explained.

The distributions obtained at lower temperatures (Figs. 7b and 7c) exhibit similar features, although they are affected by considerably larger noise with decreasing temperature due to the decreased mobility of the molecules. The most important difference from the 200 K data is that in state I the peak of the $P(U_b^{ice})$ distribution occurs around -80 kJ/mol (rather than -100 kJ/mol) at 100 K, and it is splitted to two peaks, being at about -80 kJ/mol and -60 kJ/mol at 50 K. Correspondingly, at 100 K the $P(U_b^{lat})$ distribution exhibits a much larger peak around -25 kJ/mol than at 200 K, and a rather small peak occurs also close to -50 kJ/mol. Further, at 50 K, the peak around -25 kJ/mol completely vanishes, and that at -50 kJ/mol becomes very large. These findings indicate that at these low temperatures adsorbed formamide molecules are not at all isolated from each other even at very low surface densities (state I corresponds, on average, to 3.5 and 1.5 formamide molecules per surface at 100 K and 50 K, respectively, see Tables 1 and 2), instead, they are very strongly interacting with each other even at such low surface densities. This extremely strong affinity of the formamide molecules for lateral interaction is in a clear accordance with the observed non-Langmuir nature of the adsorption isotherms, as discussed previously in this paper.

Finally, the heat of adsorption at infinitely low surface coverage, an experimentally accessible quantity can, in principle, be well estimated from the mean value of the $P(U_b^{ice})$ distribution at low enough surface density, i.e., when the adsorbed molecules are completely isolated from each other. However, in the present case we can calculate its value only in the case of I_h ice, when, in state I, the adsorbed molecules are indeed isolated from each other (see the middle panel of Fig. 7.a). For this system, the heat of adsorption at infinitely low surface density turns out to be -105.6 kJ/mol. Unfortunately, we are not aware of any experiment concerning this quantity yet. However, its measurement in the future can provide a further test of the reliability of the present results. In the case of LDA, on the other hand, we do not have the situation of completely isolated adsorbed molecules even at the lowest surface density considered, and hence the mean value of $P(U_b^{ice})$ in state I, turned out to be -99 kJ/mol, -80 kJ/mol, and -68 kJ/mol at 200 K, 100 K, and 50 K, respectively, can only serve as an upper

estimate of the heat of adsorption at infinite dilution, which becomes increasingly crude with decreasing temperature.

4. Summary and Conclusions

In this paper, we have investigated the adsorption of formamide at the surface of I_h and LDA ices under both interstellar and tropospheric conditions by computer simulation methods. The obtained adsorption isotherms revealed the ability of formamide to form multimolecular adsorption layer, the thickness of which might well (i.e., orders of magnitude) exceed the size of the simulation box. The isotherms turned out to be between types II and III according to IUPAC convention. Thus, preceding multilayer adsorption, the $\Gamma(p_{rel})$ isotherms exhibit a plateau corresponding to a rather stable adsorption layer, the range of which is getting progressively narrower with decreasing temperature. This stable layer is, however, still an unsaturated monolayer, and the building up of the outer molecular layers starts somewhat before the first layer becomes saturated. This finding indicates, in accordance with earlier results,[95,107,108] that the adsorbate-adsorbent and lateral interactions are of roughly the same magnitude. Thus, adsorbed formamide molecules are not isolated from each other even at very low surface densities, and this effect is more marked at lower temperatures. As a consequence, the isotherms exhibit non-Langmuir shape even in the pressure range that precedes multilayer adsorption. However, in spite of this non-Langmuir shape, we could estimate both the partition coefficient of formamide between the adsorption layer and the vapor phase, K (from the fit of the very low pressure part of the data), and the surface density of the saturated monolayer, Γ_{max} (from the density profile of the first layer molecules in the case of strongly multilayer adsorption). Thus, the value of K turned out to be in the order of 5×10^4, 6×10^{18}, and 10^{43} at 200 K, 100 K, and 50 K, respectively, while Γ_{max} was found to be 10.5 ± 0.7 μmol/m^2 on LDA and 9.4 μmol/m^2 on I_h ice. Due to the strong lateral association of the formamide molecules, we could only estimate the heat of adsorption at infinitely low surface coverage on I_h ice at 200 K, where it turned out to be -105.6 kJ/mol. On LDA, on the other hand, only an upper estimate of this value (being cruder at lower temperatures) was obtained, being -99 kJ/mol at 200 K, -80 kJ/mol at 100 K, and -68 kJ/mol at 50 K.

The analysis of the first molecular layer revealed that at the ice surface formamide molecules typically form four hydrogen bonds with their neighbors, and only the ratio of the water and formamide molecules among these H-bonded neighbors depend on the temperature, ice type and surface coverage. To maximize their hydrogen bonding both with surface waters and other formamides, the adsorbed formamide molecules in the first molecular layer prefer parallel as well as tilted but not twisted alignments relative to the ice surface.

In the lack of Antoine parameters that are reliable in the temperature range studied, we could only give a very crude estimate of the pressure that corresponds to a more or less saturated monolayer, however, this crude estimate is at least certainly (much) higher than the real value. Based on this (over)estimation, we found that the adsorption of formamide on LDA ice in the temperature range characteristic to the interstellar medium, and also on I_h ice at the tropospheric temperature of 200 K is a strongly preferred process, which certainly has to be taken into account in studying chemical reactivity in these environments.

Acknowledgements

The authors acknowledge financial support from the NKFIH Foundation, Hungary (project number 119732), and from CNRS in the frame of the PICS program. M. Sz. is grateful for the financial support by the János Bolyai Research Scholarship of the Hungarian Academy of Sciences (BO/00113/15/7), the New National Excellence Program of the Hungarian Ministry of Human Capacities (ÚNKP-18-4-ME/4), and also acknowledges the support provided by the European Union and the Hungarian State, co-financed by the European Regional Development Fund in the framework of the GINOP-2.3.4-15-2016-00004 project, aimed to promote the cooperation between the higher education and the industry. The GITDA (Governmental Information-Technology Development Agency, Hungary) is also gratefully acknowledged for allocating computing resources used in this work.

References

(1) Ge, X.; Wexler, A. S.; Clegg, S. L. Atmospheric Amines - Part I. A Review. *Atmos. Environ.* **2011**, *45*, 524−546.

(2) Yi, Y.; Zhou, X.; Xue, L.; Wang, W. Air Pollution: Formation of Brown, Lighting-Absorbing, Secondary Organic Aerosols by Reaction of Hydroxyacetone and Methylamine. *Environ. Chem. Lett.* **2018**, *16*, 1083–1088.

(3) Cheng, Y.; Li, S.; Leithead, A. Chemical Characteristics and Origins of Nitrogen-Containing Organic Compounds in PM2.5 Aerosols in the Lower Fraser Valley. *Environ. Sci. Technol.* **2006**, *40*, 5846−5852.

(4) Laskin, A.; Smith, J. S.; Laskin, J. Molecular Characterization of Nitrogen-Containing Organic Compounds in Biomass Burning Aerosols Using High-Resolution Mass Spectrometry. *Environ. Sci. Technol.* **2009**, *43*, 3764−3771.

(5) Raja, S.; Raghunathan, R.; Kommalapati, R. R.; Shen, X.; Collett, J. L., Jr.; Valsaraj, K. T. Organic Composition of Fogwater in the Texas−Louisiana Gulf Coast Corridor. *Atmos. Environ.* **2009**, *43*, 4214−4222.

(6) Zhu, L.; Schade, G. W.; Nielsen, C. J. Real-Time Monitoring of Emissions from Monoethanolamine-Based Industrial Scale Carbon Capture Facilities. *Environ. Sci. Technol.* **2013**, *47*, 14306−14314.

(7) Borduas, N.; da Silva, G.; Murphy, J. G.; Abbatt, J. P. D. Experimental and Theoretical Understanding of the Gas Phase Oxidation of Atmospheric Amides with OH Radicals: Kinetics, Products, and Mechanisms. *J. Phys. Chem. A* **2015**, *119*, 4298–4308

(8) Chakir, A.; Solignac, G.; Mellouki, A.; Daumont, D.; Gas Phase, UV Absorption Cross-Sections for a Series of Amides. *Chem. Phys. Letters* **2005**, *404*, 74−78.

(9) Barnes, I.; Solignac, G.; Mellouki, A.; Becker, K. H. Aspects of the Atmospheric Chemistry of Amides. *Chem. Phys. Chem.* **2010**, *11*, 3844–3857.

(10) Bunkan, A. J. C.; Mikoviny, T.; Nielsen, C. J.; Wisthaler, A.; Zhu, L. Experimental and Theoretical Study of the OH-Initiated Photo-oxidation of Formamide. *J. Phys. Chem. A* **2016**, *120*, 1222–1230.

(11) Bunkan, A. J. C.; Hetzler, J.; Mikoviny, T.; Wisthaler, A.; Nielsen C. J.; Olzmann, M. Aspects of the Atmospheric Chemistry of Amides. *Phys. Chem. Chem. Phys.* **2015**, *17*, 7046-7059.

(12) Borduas, N.; Abbatt, J. P. D.; Murphy, J. G.; So, S.; da Silva, G. Gas-Phase Mechanisms of the Reactions of Reduced Organic Nitrogen Compounds with OH Radicals. *Environ. Sci. Technol.* **2016**, *50*, 11723–11734.

(13) Šponer, J. E.; Šponer, J.; Nováková, O.; Brabec, V.; Šedo, O.; Zdráhal, Z.; Costanzo, G.; Pino, S.; Saladino, R.; Di Mauro, E. Emergence of the First Catalytic Oligonucleotides in a Formamide-Based Origin Scenario. *Chem. Eur. J.* **2016**, *22*, 3572–3586.

(14) Saladino, R.; Crestini, C.; Pino, S.; Costanzo, G.; Di Mauro, E. Formamide and the Origin of Life. *Phys. Life Rev.* **2012**, *9*, 84–104.

(15) Rotelli, L.; Trigo-Rodríguez, J. M.; Moyano-Cambero, C. E.; Carota, E.; Botta, L.; Di Mauro, E.; Saladino, R.; Chyba, C. F.; Oró, J.; Mojzsis, S. J.; et al. The Key Role of Meteorites in the Formation of Relevant Prebiotic Molecules in a Formamide/Water Environment. *Sci. Rep.* **2016**, *6*, 38888-1-7

(16) Szőri, M.; Jójárt, B.; Izsák, R.; Szori, K.; Csizmadia, I. G.; Viskolcz, B. Chemical Evolution of Biomolecule Building Blocks. Can Thermodynamics Explain the Accumulation of Glycine in the Prebiotic Ocean? *Phys. Chem. Chem. Phys.* **2011**, *13*, 7449–7458.

(17) Pietrucci, F.; Saitta, A. M. Formamide Reaction Network in Gas Phase and Solution via a Unified Theoretical Approach: Toward a Reconciliation of Different Prebiotic Scenarios. *Proc. Natl. Acad. Sci.* **2015**, *112*, 15030–15035.

(18) Saitta, A. M.; Saija, F. Miller Experiments in Atomistic Computer Simulations. *Proc. Natl. Acad. Sci.* **2014**, *111*, 13768–13773.

(19) Botta, L., Saladino, R., Bizzarri, B. M., Cobucci-Ponzano, B., Iacono, R., Avino, R., Caliro, S., Carandente, A., Lorenzini, F., Tortora, A., Di Mauro, E., Moracci, M., Formamide-Based Prebiotic Chemistry in the Phlegrean Fields. *Adv. Space Res.* **2018**, *62*, 2372-2379.

(20) Matthews, C. N. In *Origins: Genesis, Evolution and Diversity of Life* (Series: Cellular Origin and Life in Extreme Habitats and Astrobiology, Volume 6); Seckbach, J.; Ed; Kluwer: Dordrecht, 2004, p. 121-135.

(21) Minard, R. D.; Matthews, C. N. HCN World: Establishing Proteininucleic Acid Life via Hydrogen Cyanide Polymers. *Abstr. Pap. Am. Chem. Soc.* **2004,** *228*, U963-U963.

(22) Saladino, R.; Crestini, C.; Ciciriello, F.; Costanzo, G.; Di Mauro, E. Formamide Chemistry and the Origin of Informational Polymers. *Chem. Biodivers.* **2007**, *4*, 694–720.

(23) Kua, J.; Thrush, K. L. HCN, Formamidic Acid, and Formamide in Aqueous Solution: A Free Energy Map. *J. Phys. Chem. B* **2016**, *120*, 8175–8185.

(24) Sanchez, R. A.; Ferris, J. P.; Orgel, L. E. Studies in Prebiotic Synthesis. II. Synthesis of Purine Precursors and Amino Acids from Aqueous Hydrogen Cyanide. *J. Mol. Biol.* **1967**, *30*, 223–253.

(25) Fábián, B.; Szőri, M.; Jedlovszky, P. Floating Patches of HCN at the Surface of Their Aqueous Solutions – Can They Make "HCN World" Plausible? *J. Phys. Chem. C* **2014**, *118*, 21469–21482.

(26) Szőri, M.; Jedlovszky, P. Adsorption of HCN at the Surface of Ice: A Grand Canonical Monte Carlo Simulation Study. *J. Phys. Chem. C* **2014**, *118*, 3599–3609.

(27) Menor-Salván, C.; Marín-Yaseli, M. R. Prebiotic Chemistry in Eutectic Solutions at the Water–Ice Matrix. *Chem. Soc. Rev.*, **2012**, *41*, 5404–5415.

(28) Costanzo, G., Saladino, R., Crestini, C., Ciciriello, F., and Di Mauro, E. Formamide as the Main Building Block in the Origin of Nucleic Acids. *BMC Evol. Biol.* **2007**, *7 (Suppl. 2)*, S1-1-8.

(29) Marín-Yaseli, M. R.; Moreno, M.; de la Fuente, J. L.; Briones, C.; Ruiz-Bermejo, M. Experimental Conditions Affecting the Kinetics of Aqueous HCN Polymerization as Revealed by UV–VIS Spectroscopy. *Spectrochim. Acta A* **2018**, *191*, 389–397.

(30) Flygare, W. H.; Benson, R. C.; Tigelaar, H. L.; Rubin, R. H.; Swenson, G. W. In *Molecules in the Galactic Environment*; Gordon, M. A., Ed.; Wiley: New York, 1973, pp. 173–179.

(31) Gottlieb, C. A.; Palmer, P.; Rickard, L. J.; Zuckerman, B. Studies of Interstellar Formamide. *Astrophys. J.* **1973**, 182, 699–710.

(32) Adande, G. R.; Woolf, N. J.; Ziurys, L. M. Observations of Interstellar Formamide: Availability of a Prebiotic Precursor in the Galactic Habitable Zone. *Astrobiology* **2013**, *13*, 439-453.

(33) Schutte, W. A.; Boogert, A. C. A.; Tielens, A.; Whittet, D. C. B.; Gerakines, P. A.; Chiar, J. E.; Ehrenfreund, P.; Greenberg, J. M.; van Dishoeck, E. F.; de Graauw, T.

Weak Ice Absorption Features at 7.24 and 7.41 MU M in the Spectrum of the Obscured Young Stellar Object W 33A. *Astron. Astrophys.* **1999**, *343*, 966–976.

(34) Solomon, P. M. (1973). Interstellar Molecules. *Physics Today* **1973**, *26*, 32–40.

(35) Bockelee-Morvan, D.; Lis, D. C.; Wink, J. E.; Despois, D.; Crovisier, J.; Bachiller, R.; Benford, D. J.; Biver, N.; Colom, P.; Davies, J. K.; Gerard, E.; Germain, B.; Houde, M.; Mehringer, D.; Moreno, R.; Paubert, G.; Phillips, T. G.; Rauer, H. New Molecules Found in Comet C/1995 O1 (Hale-Bopp) - Investigating the Link Between Cometary and Interstellar Material. *Astron. Astrophys.* **2000**, 353, 1101–1114.

(36) Despois, D.; Crovisier, J.; Bockele-Morvan, D.; Biver, N. In *Proceedings of the Second European Workshop on Exo-Astrobiology, ESA-SP, Vol. 518*; Lacoste, H., Ed.; Noordwijk: ESA Publications: Nordwijk, 2002, pp. 123–127.

(37) Lis, D. C.; Mehringer, D. M.; Benford, D.; Gardner, M.; Phillips, T. G.; Bockelee-Morvan, D.; Biver, N.; Colom, P.; Crovisier, J.; Despois, D.; Rauer, H. New Molecular Species in Comet C/1995O1(Hale-Bopp) Observed with the Caltech Submillimeter Observatory. *Earth Moon Planets* **1997**, *78*, 13–20.

(38) Hudson, R. L.; Moore, M. H. Reactions of Nitriles in Ices Relevant to Titan, Comets, and the Interstellar Medium: Formation of Cyanate Ion, Ketenimines, and Isonitriles". *Icarus* **2004**, 172, 466–478.

(39) Rimola, A.; Skouteris, D.; Balucani, N.; Ceccarelli, C.; Enrique-Romero, J.; Taquet, V.; Ugliengo, P. Can Formamide Be Formed on Interstellar Ice? An Atomistic Perspective. *ACS Earth Space Chem.*, **2018**, *2*, 720–734.

(40) Gao, Y.; Qin, Z.; Guan, L.; Wang, X.; Chen G. Z. Organoaqueous Calcium Chloride Electrolytes for Capacitive Charge Storage in Carbon Nanotubes at Sub-Zero-Temperatures. *Chem. Commun.* **2015,** *51*, 10819-10822.

(41) Carota, E.; Botta, G.; Rotelli, L.; Di Mauro, E.; Saladino, R. Current Advances in Prebiotic Chemistry Under Space Conditions. *Curr. Org. Chem.* **2015**, *19*, 1963-1979.

(42) Mispelaer, F.; Theule, P.; Aouididi, H.; Noble, J.; Duvernay, F.; Danger, G.; Roubin, P.; Morata, O.; Hasegawa, T.; Chiavassa, T.; Diffusion Measurements of CO, HNCO, H_2CO, and NH_3 in Amorphous Water Ice. *Astron. Astrophys.* **2013,** *555*, A13.

(43) Cottin, H.; Gazeau, M. C.; Raulin, F. Cometary Organic Chemistry: A Review from Observations Numerical and Experimental Simulations. *Planet. Space Sci.* **1999,** *47*, 1141–1162.

(44) Wakelam, V.; Loison, J. C.; Mereau, R.; Ruaud, M. Binding Energies: New Values and Impact on the Efficiency of Chemical Desorption. *Mol. Astrophys.* **2017**, *6*, 22-35.

(45) Chaabouni, H.; Diana, S.; Nguyen, T.; Dulieu, F. Thermal Desorption of Formamide and Methylamine from Graphite and Amorphous Water Ice Surfaces. *Astron. Astrophys.* **2018**, *612*, A47.

(46) Allen, M. P.; Tildesley, D. J. *Computer Simulation of Liquids*; Clarendon: Oxford, 1987.

(47) Adams, D. J. Grand Canonical Ensemble Monte Carlo for a Lennard-Jones Fluid. *Mol. Phys.* **1975,** *29*, 307-311.

(48) Rutkai, G.; Kristóf, T. Molecular Simulation Study of Intercalation of Small Molecules in Kaolinite. *Chem. Phys. Letters* **2008**, *462*, 269-274.

(49) Croteau, T.; Bertram, A. K.; Patey, G. N. Adsorption and Structure of Water on Kaolinite Surfaces: Possible Insight into Ice Nucleation from Grand Canonical Monte Carlo Calculations. *J. Phys. Chem. A* **2008,** *112*, 10708-10712.

(50) Jameson, C. J.; Jameson, K.; Baello, B. I.; Lim, H. M. Grand Canonical Monte Carlo Simulations of the Distribution and Chemical Shifts of Xenon in the Cages of Zeolite NaA. 1. Distribution and Xe-129 Chemical Shifts. *J. Chem. Phys.* **1994,** *100*, 5965-5976.

(51) Jameson, C. J.; Jameson, K.; Lim, H. M.; Baello, B. I. Grand Canonical Monte Carlo Simulations of the Distribution and Chemical Shifts of Xenon in the Cages of Zeolite NaA. 2. Structure of the Adsorbed Fluid. *J. Chem. Phys.* **1994,** *100*, 5977-5987.

(52) Smit, B. Grand Canonical Monte Carlo Simulations of Chain Molecules: Adsorption Isotherms of Alkanes in Zeolites. *Mol. Phys.* **1995,** *85*, 153-172.

(53) Pellenq, R. J. M.; Tavitian, B.; Espinat, D.; Fuchs, A. H. Grand Canonical Monte Carlo Simulations of Adsorption of Polar and Nonpolar Molecules in NaY Zeolite. *Langmuir* **1996,** *12*, 4768-4783.

(54) Macedonia, M. D.; Maginn, E. J. Pure and Binary Component Sorption Equilibria of Light Hydrocarbons in the Zeolite Silicalite from Grand Canonical Monte Carlo Simulations. *Fluid Phase Equil.* **1999,** *158-160*, 19-27.

(55) Rutkai, G.; Csányi, É.; Kristóf, T. Prediction of Adsorption Equilibria of Water-Methanol Mixtures in Zeolite NaA by Molecular Simulation. *Mol. Simul.* **2006,** *32*, 869-875.

(56) Kristóf, T.; Csányi, É.; Rutkai, G. Prediction of Adsorption and Separation of Water-Alcohol Mixtures with Zeolite NaA. *Microporous Mesoporous Mat.* **2008,** *114*, 455-464.

(57) Puibasset, J.; Pellenq, R. J. M. Water Adsorption on Hydrophilic Mesoporous and Place Silica Substrates: a Grand Canonical Monte Carlo Simulation Study. *J. Chem. Phys.* **2003,** *118*, 5613-5622.

(58) Puibasset, J.; Pellenq, R. J. M. Water Adsorption in Disordered Mesoporous Silica (Vycor) at 300 K and 650 K : A Grand Canonical Monte Carlo Simulation Study of Hysteresis. *J. Chem. Phys.* **2005,** *122*, 094704.

(59) Daub, C. D.; Patey G. N.; Jack, D. B.; Sallabi A. K. Monte Carlo Simulations of the Adsorption of CO_2 on the MgO(100) Surface. *J. Chem. Phys.* **2006,** *124*, 114706.

(60) Tombácz, E.; Hajdú, A.; Illés, E.; László, K.; Garberoglio, G.; Jedlovszky, P. Water in Contact with Magnetite Nanoparticles, as Seen from Experiments and Computer Simulations. *Langmuir* **2009,** *25*, 13007-13014.

(61) Jedlovszky, P.; Partay, L.; Hoang, P. N. M.; Picaud, S.; von Hessberg, P.; Crowley, J. N. Determination of the Adsorption Isotherm of Methanol on the Surface of Ice. An Experimental and Grand Canonical Monte Carlo Simulation Study. *J. Am. Chem. Soc.* **2006**, *128*, 15300-15309.

(62) Hantal, Gy.; Jedlovszky, P.; Hoang, P.N.M.; Picaud, S. Investigation of the Adsorption Behavior of Acetone at the Surface of Ice. A Grand Canonical Monte Carlo Simulation Study. *Phys. Chem. Chem. Phys.* **2008**, *10*, 6369-6380.

(63) Jedlovszky, P.; Hantal, Gy.; Neuróhr, K.; Picaud, S.; Hoang, P. N. M.; von Hessberg, P.; Crowley, J. N. Adsorption Isotherm of Formic Acid on The Surface of Ice, as Seen from Experiments and Grand Canonical Monte Carlo Simulation. *J. Phys. Chem. C* **2008,** *112*, 8976-8987.

(64) Petitjean, M.; Hantal, Gy.; Chauvin, C.; Mirabel, P.; Le Calvé, S.; Hoang, P. N. M.; Picaud, S.; Jedlovszky, P. Adsorption of Benzaldehyde at the Surface of Ice, Studied by Experimental Method and Computer Simulation. *Langmuir* **2010,** *26*, 9596-9606.

(65) Mészár, Zs. E.; Hantal, Gy.; Picaud, S.; Jedlovszky, P. Adsorption of Aromatic Hydrocarbon Molecules at the Surface of Ice, As Seen by Grand Canonical Monte Carlo Simulation. *J. Phys. Chem. C* **2013,** *117*, 6719-6729.

(66) Sumi, I.; Picaud, S.; Jedlovszky, P. Adsorption of Methylene Fluoride and Methylene Chloride at the Surface of Ice under Tropospheric Conditions. A Grand Canonical Monte Carlo Simulation Study. *J. Phys. Chem. C* **2015,** *119*, 17243-17252.

(67) Sumi, I.; Fábián, B.; Picaud, S.; Jedlovszky, P. Adsorption of Fluorinated Methane Derivatives at the Surface of Ice under Tropospheric Conditions, As Seen from Grand Canonical Monte Carlo Simulations. *J. Phys. Chem. C* **2016,** *120*, 17386-17399.

(68) Szentirmai, V.; Szőri, M.; Picaud, S.; Jedlovszky, P. Adsorption of Methylamine at the Surface of Ice. A Grand Canonical Monte Carlo Simulation Study *J. Phys. Chem. C* **2016,** *120*, 23480-23489.

(69) Sumi, I.; Picaud, S.; Jedlovszky, P. Adsorption of Chlorinated Methane Derivatives at the Ice Surface: A Grand Canonical Monte Carlo Simulation Study. *J. Phys. Chem. C* **2017,** *121*, 7782-7793.

(70) Horváth, R. A.; Hantal, Gy.; Picaud, S.; Szőri, M.; Jedlovszky, P. Adsorption of Methylamine on Amorphous Ice under Interstellar Conditions. A Grand Canonical Monte Carlo Simulation Study. *J. Phys. Chem. A* **2018,** *122*, 3398-3412.

(71) Samios, S.; Stubos, A. K.; Kanellopoulos, N. K.; Cracknell, R. F.; Papadopoulos, G. K.; Nicholson, D. Determination of Micropore Size Distribution from Grand Canonical Monte Carlo Simulations and Experimental CO_2 Isotherm Data. *Langmuir* **1997,** *13*, 2795-2802.

(72) Muller, E. A.; Hung, F. R.; Gubbins, K. E. Adsorption of Water Vapor-Methane Mixtures on Activated Carbons. *Langmuir* **2000,** *16*, 5418-5424.

(73) Challa, S. R.; Sholl, D. S.; Johnson, J. K. Adsorption and Separation of Hydrogen Isotopes in Carbon Nanotubes: Multicomponent Grand Canonical Monte Carlo Simulations. *J. Chem. Phys.* **2002,** *116*, 814-824.

(74) Striolo, A.; Chialvo, A. A.; Gubbins, K. E.; Cummings, P. T. Water in Carbon Nanotubes: Adsorption Isotherms and Thermodynamic Properties from Molecular Simulation. *J. Chem. Phys.* **2005,** *122*, 234712.

(75) Moulin, F.; Picaud, S.; Hoang, P. N. M.; Jedlovszky, P. Grand Canonical Monte Carlo Simulation of the Adsorption Isotherms of Water Molecules on a Model Soot Particle *J. Chem. Phys.* **2007,** *127,* 164719.

(76) Hantal, Gy.; Picaud, S.; Hoang, P. N. M.; Voloshin, V. P.; Medvedev, N. N.; Jedlovszky, P. Water Adsorption Isotherms on Porous Onionlike Carbonaceous Particles. Simulations with the Grand Canonical Monte Carlo Method. *J. Chem. Phys.* **2010,** *133,* 144702.

(77) Firlej, L.; Kuchta, B.; Lazarewicz, A.; Pfeifer, P. Increased H_2 Gravimetric Storage Capacity in Truncated Carbon Slit Pores Modeled by Grand Canonical Monte Carlo. *Carbon* **2013,** *53,* 208-215.

(78) Szőri, M.; Jedlovszky, P.; Roeselová, M. Water Adsorption on Hydrophilic and Hydrophobic Self-Assembled Monolayers as Proxies For Atmospheric Surfaces. A Grand Canonical Monte Carlo Simulation Study. *Phys. Chem. Chem. Phys.* **2010,** *12*, 4604-4616.

(79) Szőri, M.; Roeselová, M.; Jedlovszky, P. Surface Hydrophilicity-Dependent Water Adsorption on Mixed Self-Assembled Monolayers of C_7-CH_3 and C_7-COOH residues. A Grand Canonical Monte Carlo Simulation Study. *J. Phys. Chem. C* **2011,** *115*, 19165-19177.

(80) Jung, D. H.; Kim, D.; Lee, T. B.; Choi, S. B.; Yoon, J. H.; Kim, J.; Choi, K.; Choi, S. H. Grand Canonical Monte Carlo Simulation Study on the Catenation Effect on Hydrogen Adsorption onto the Interpenetrating Metal-Organic Frameworks. *J. Phys. Chem. B* **2006,** *110,* 22987-22990.

(81) Garberoglio, G. Computer Simulation of the Adsorption of Light Gases in Covalent Organic Frameworks. *Langmuir* **2007,** *23,* 12154-12158.

(82) Ramsahye, N. A.; Maurin, G.; Bourelly, S.; Llewellyn, P. L.; Devic, T.; Serre, C.; Loiseau, T.; Ferey, G. Adsorption of CO_2 in Metal Organic Frameworks of Different Metal Centres: Grand Canonical Monte Carlo Simulations Compared to Experiments. *Adsorption* **2007,** *13*, 461-467.

(83) Resat, H.; Mezei, M. Grand Canonical Monte Carlo Simulation of Water Positions in Crystal Hydrates. *J. Am. Chem. Soc.* **1994**, *116*, 7451-7452.

(84) Tanaka, H. A Novel Approach to the Stability of Clathrate Hydrates: Grand Canonical Monte Carlo Simulation. *Fluid Phase Equilib.* **1998,** *144*, 361−368.

(85) Sizov, V. V.; Piotrovskaya, E. M. Computer Simulation of Methane Hydrate Cage Occupancy. *J. Phys. Chem. B* **2007,** *111*, 2886−2890.

(86) Papadimitriou, N. I.; Tsimpanogiannis, I. N.; Papaioannou, A. Th.; Stubos, A. K. Evaluation of the Hydrogen-Storage Capacity of Pure H2 and Binary H2-THF Hydrates with Monte Carlo Simulations. *J. Phys. Chem. C* **2008,** *112*, 10294−10302.

(87) Matsuo, M.; Takii, Y.; Matsumoto, M.; Tanaka, H. On the Occupancy of Carbon Dioxide Clathrate Hydrates: Grandcanonical Monte Carlo Simulations. *J. Phys. Soc. Japan* **2012,** *81*, SA027-1-6.

(88) Lasich, M.; Mohammadi, A. H.; Bolton, K.; Vrabec, J.; Ramjugernath, D. Phase Equilibria of Methane Clathrate Hydrates from Grand Canonical Monte Carlo simulation. *Fluid Phase Equilib.* **2014,** *369*, 47-54.

(89) Papadimitriou, N. I.; Tsimpanogiannis, I. N.; Economou, I. G.; Stubos, A. K. Storage of H_2 in Clathrate Hydrates: Evaluation of Different Force-Fields used in Monte Carlo Simulations. *Mol. Phys.* **2017,** *115*, 1274-1285.

(90) Fábián, B.; Picaud, S.; Jedlovszky, P.; Guilbert-Lepoutre, A.; Moussis, O. Ammonia Clathrate Hydrate As Seen from Grand Canonical Monte Carlo Simulations. *ACS Earth and Space Chemistry* **2018,** *2*, 521-531.

(91) Patt, A.; Simon, J. M.; Picaud, S.; Salazar, J. M. A Grand Canonical Monte Carlo Study of the N_2, CO, and Mixed N_2-CO Clathrate Hydrates. *J. Phys. Chem. C* **2018**, *122*, 18432-18444.

(92) Dawley, M. M.; Pirim, C.; Orlando, T. M. Thermal Processing of Formamide Ices on Silicate Grain Analogue. *J. Phys. Chem. A* **2014**, *118*, 1220-1227.

(93) Berendsen, H. J. C.; Grigera, J. R.; Straatsma, T. The Missing Term in Effective Pair Potentials. *J. Phys. Chem.* **1987,** *91*, 6269-6271.

(94) Bjelkmar, P.; Larsson, P.; Cuendet, M. A.; Bess, B.; Lindahl, E. Implementation of the CHARMM Force Field in GROMACS: Analysis of Protein Stability Effects from Correction Maps, Virtual Interaction Sites, and Water Models. *J. Chem. Theory Comput.* **2010**, *6*, 459-466.

(95) Kiss, B.; Fábián, B.; Idrissi, A.; Szőri, M.; Jedlovszky, P. Miscibility and Thermodynamics of Mixing of Different Models of Formamide and Water in Computer Simulation. *J. Phys. Chem. B* **2017,** *121*, 7147-7155, erratum: *J. Phys. Chem. B* **2017,** *121,* 9319-9319.

(96) Mezei, M. *MMC: Monte Carlo Program for Simulation of Molecular Assemblies.* URL: http://inka.mssm.edu/~mezei/mmc.

(97) Mezei, M. A Cavity-Biased (T, V, μ) Monte Carlo Method for the Computer-Simulation of Fluids. *Mol. Phys.* **1980,** *40,* 901-906.

(98) Mezei, M. Grand Canonical Ensemble Monte Carlo Study of Dense Liquid Lennard-Jones, Soft Spheres and Water. *Mol. Phys.* **1987,** *61,* 565-582. Erratum: **1989,** *67,* 1207-1208.

(99) Metropolis, N.; Rosenbluth, A. W.; Rosenbluth, M. N.; Teller, A. H.; Teller, E. Equation of State Calculations by Fast Computing Machines *J. Chem. Phys.* **1953,** *21* 1087-1093.

(100) Chacón, E.; Tarazona, P. Intrinsic Profiles Beyond the Capillary Wave Theory: A Monte Carlo Study. *Phys Rev. Letters* **2003,** *91,* 166103-1-4.

(101) Chowdhary, J.; Ladanyi, B. M. Water-Hydrocarbon Interfaces: Effect of Hydrocarbon Branching on Interfacial Structure. *J. Phys. Chem. B.* **2006,** *110,* 15442-15453.

(102) Jorge, M.; Cordeiro, M. N. D. S. Intrinsic Structure and Dynamics of the Water/Nitrobenzene Interface. *J. Phys. Chem. C.* **2007,** *111*, 17612-17626.

(103) Pártay, L. B.; Hantal, Gy.; Jedlovszky, P.; Vincze, Á.; Horvai, G. A New Method for Determining the Interfacial Molecules and Characterizing the Surface Roughness in Computer Simulations. Application to the Liquid–Vapor Interface of Water. *J. Comp. Chem.* **2008,** *29,* 945-956.

(104) Jorge, M.; Jedlovszky, P.; Cordeiro, M. N. D. S. A Critical Assessment of Methods for the Intrinsic Analysis of Liquid Interfaces. 1. Surface Site Distributions. *J. Phys. Chem. C.* **2010,** *114*, 11169-11179.

(105) Wilard, A. P.; Chandler, D. Instantaneous Liquid Interfaces. *J. Phys. Chem. B.* **2010,** *114*, 1954-1958.

(106) Sega, M.; Kantorovich, S.; Jedlovszky, P; Jorge, M. The Generalized Identification of Truly Interfacial Molecules (ITIM) Algorithm for Nonplanar Interfaces. *J. Chem. Phys.* **2013,** *138,* 044110-1-10.

(107) Puhovski, Y. P.; Rode, B. M. Molecular Dynamics Simulations of Aqueous Formamide Solution. 2. Dynamics of Solvent Molecules. *J. Chem. Phys.* **1995,** *102*, 2920-2927.

(108) Elola, M. D.; Ladanyi, B. M. Intermolecular Polarizability Dynamics of Aqueous Formamide Liquid Mixtures Studied by Molecular Dynamics Simulations. *J. Chem. Phys.* **2007,** *126*, 084504-1-13.

(109) Langmuir, I. The Constitution and Fundamental Properties of Solids and Liquids. Part I: Solids. *J. Am. Chem. Soc.* **1916,** *38*, 2221-2295.

(110) Shaw, D. J. *Introduction to Colloid and Surface Chemistry*, Butterworths: London, 1980.

(111) Thomson, G. W. The Antoine Equation for Vapor-Pressure Data. *Chem. Rev.* **1946,** *38*, 1-39.

(112) Stull, D. R. Vapor Pressure of Pure Substances. Organic and Inorganic Compounds. *Ind. Eng. Chem.* **1947,** *39*, 517-540.

(113) *NIST Chemistry WebBook, SRD 69.* URL: http://webbook.nist.gov/cgi/cbook.cgi?ID=C75127&Mask=4&Type=ANTOINE&Plot=on (accessed in 06/12/2018).

(114) Sarkar, C.; Sinha, V.; Kumar, V.; Rupakheti, M.; Panday, A.; Mahata, K. S.; Rupakheti, D.; Kathayat, B.; Lawrence, M. G. Overview of VOC Emissions and Chemistry from PTR-TOF-MS Measurements during the SusKat-ABC Campaign: High Acetaldehyde, Isoprene and Isocyanic Acid in Wintertime Air of the Kathmandu Valley. *Atmos. Chem. Phys.*, **2016**, *16*, 3979–4003.

(115) Jedlovszky, P.; Vincze, Á.; Horvai, G. New Insight into the Orientational Order of Water Molecules at the Water/1,2-Dichloroethane Interface: A Monte Carlo Simulation Study. *J. Chem. Phys.* **2002,** *117*, 2271-2280.

(116) Jedlovszky, P.; Vincze, Á.; Horvai, G. Full Description of the Orientational Statistics of Molecules Near to Interfaces. Water at the Interface with CCl_4. *Phys. Chem. Chem. Phys.* **2004,** *6*, 1874-1879.

(117) Kiss, B.; Fábián, B.; Idrissi, A.; Szőri, M.; Jedlovszky, P. Investigation of the Liquid-Vapor Interface of Water-Formamide Mixtures by Computer Simulation and Intrinsic Surface Analysis. *J. Phys. Chem. C* **2018,** *122*, 19639-19651.

Tables

Table 1. Data of the Adsorption Isotherm of Formamide on LDA Ice at 50 K, as Obtained from the Simulations. The μ Value Corresponding to the Point of Condensation Is Also Indicated (Bold Characters).

μ/kJ mol^{-1}	$\langle N \rangle$	p/p_0	Γ/μmol m^{-2}
-63.54[a]	3.020	3.66×10^{-55}	0.178
-62.29	9.017	7.35×10^{-54}	0.535
-61.46	11.03	5.43×10^{-53}	0.654
-60.21	13.20	1.09×10^{-51}	0.773
-58.13	32.52	1.62×10^{-49}	1.90
-56.06	37.34	2.40×10^{-47}	2.20
-53.98[b]	60.28	3.57×10^{-45}	3.58
-51.90	68.07	5.29×10^{-43}	4.04
-49.82	81.12	7.85×10^{-41}	4.81
-48.99[c]	115.4	5.80×10^{-40}	6.83
-48.57	515.2	1.58×10^{-39}	30.6
-48.16	896.6	4.29×10^{-39}	53.3
-47.74[d]	907.8	1.17×10^{-38}	54.0
-46.91	910.2	8.61×10^{-38}	54.1
-46.08	912.1	6.36×10^{-37}	54.2
-45.25	906.0	4.70×10^{-36}	53.8
-11.432		**1.000**	

[a]state I [b]state II [c]state III [d]state IV

Table 2. Data of the Adsorption Isotherm of Formamide on LDA Ice at 100 K, as Obtained from the Simulations. The μ Value Corresponding to the Point of Condensation Is Also Indicated (Bold Characters).

μ/kJ mol^{-1}	$\langle N \rangle$	p/p_0	Γ/μmol m^{-2}
-69.74[a]	7.011	3.60×10^{-25}	0.416
-67.25	7.548	7.22×10^{-24}	0.449
-65.59	9.103	5.34×10^{-23}	0.535
-63.92	10.40	3.94×10^{-22}	0.618
-63.09	17.01	1.07×10^{-22}	1.01
-61.43	25.02	7.92×10^{-21}	1.49
-60.18	28.01	3.55×10^{-20}	1.66
-58.93	37.95	1.59×10^{-19}	2.26
-57.27[b]	57.86	1.18×10^{-18}	3.44
-56.02	75.13	5.27×10^{-18}	4.46
-54.78	86.83	2.36×10^{-17}	5.16
-53.95[c]	104.1	6.42×10^{-17}	6.18
-53.11	221.9	1.74×10^{-16}	13.2
-51.45[d]	894.0	1.29×10^{-15}	53.1
-49.79	895.1	9.52×10^{-15}	53.2
-48.54	896.5	4.27×10^{-14}	53.3
-47.29	898.2	1.91×10^{-13}	53.4
-22.947		**1.000**	

[a]state I [b]state II [c]state III [d]state IV

Table 3. Data of the Adsorption Isotherm of Formamide on LDA Ice at 200 K, as Obtained from the Simulations. The μ Value Corresponding to the Point of Condensation Is Also Indicated (Bold Characters).

μ/kJ mol^{-1}	$\langle N \rangle$	p/p_0	Γ/μmol m^{-2}
-76.36	0.0021	7.93×10^{-10}	1.25×10^{-4}
-73.04	0.0443	5.86×10^{-9}	2.63×10^{-3}
-70.21	1.028	3.21×10^{-8}	6.11×10^{-2}
-68.05	2.086	1.18×10^{-7}	0.124
-64.73[a]	9.434	8.70×10^{-7}	0.561
-62.73	24.10	2.89×10^{-6}	1.43
-61.90	41.68	4.76×10^{-6}	2.48
-61.40[b]	50.22	6.43×10^{-6}	2.98
-60.57	57.58	1.06×10^{-5}	3.42
-59.74	93.25	1.75×10^{-5}	5.54
-58.91[c]	118.29	2.88×10^{-5}	7.03
-58.07	338.19	4.75×10^{-5}	20.1
-57.24	872.0	7.83×10^{-5}	51.8
-56.41[d]	878.0	1.29×10^{-4}	52.2
-54.75	896.1	3.51×10^{-4}	53.2
-53.09	901.6	9.54×10^{-4}	53.6
-41.521		**1.000**	

[a]state I [b]state II [c]state III [d]state IV

Table 4. Data of the Adsorption Isotherm of Formamide on I_h Ice at 200 K, as Obtained from the Simulations. The μ Value Corresponding to the Point of Condensation Is Also Indicated (Bold Characters).

μ/kJ mol^{-1}	$\langle N \rangle$	p/p_0	Γ/μmol m^{-2}
-78.03	0.0002	2.92×10^{-10}	1.19×10^{-5}
-76.36	0.0008	7.93×10^{-10}	4.75×10^{-5}
-73.04	0.0075	5.86×10^{-9}	4.46×10^{-4}
-69.71	0.0679	4.33×10^{-8}	4.03×10^{-3}
-67.22	1.322	1.94×10^{-7}	7.86×10^{-2}
-66.39	2.307	3.20×10^{-7}	0.137
-64.73[a]	5.635	8.70×10^{-7}	0.335
-63.06	11.09	2.36×10^{-6}	0.659
-61.40[b]	42.57	6.43×10^{-6}	2.53
-60.57	54.67	1.06×10^{-5}	3.25
-59.74	112.3	1.75×10^{-5}	6.67
-58.91[c]	119.8	2.88×10^{-5}	7.12
-58.07	127.6	4.75×10^{-5}	7.58
-57.41	136.6	7.08×10^{-5}	8.12
-56.74	771.0	1.06×10^{-4}	45.8
-56.41[d]	748.1	1.29×10^{-4}	44.5
-55.91	761.4	1.74×10^{-4}	45.2
-55.25	768.0	2.60×10^{-4}	45.6
-54.75	770.9	3.51×10^{-4}	45.8
-41.521		**1.000**	

[a]state I [b]state II [c]state III [d]state IV

Figure Legend

Figure 1. Equilibrium snapshots of the system at 50K, both from top (left column) and side (right column) view, as obtained at four different chemical potential values from our simulations. Water O atoms are shown by red spheres, first layer formamide molecules (as determined by the ITIM method) are shown by blue, while outer formamide molecules by yellow color, respectively.

Figure 2. Adsorption isotherms of formamide, in the form of number of adsorbed molecules vs. chemical potential, at the surface of I_h ice at 200 K (black open symbols) as well as at the surface of LDA ice (full symbols) at 200 K (black), 100 K (red), and 50 K (green), as obtained from our simulations. The lines connecting the points are just guides to the eye. The state points at which sample configurations have been dumped for detailed analyses are marked by the arrows (see the text). The inset shows the temperature dependence of the chemical potential corresponding to the point of condensation. Black circles: simulation results, red line: straight line fitted to these data.

Figure 3. Adsorption isotherms of formamide, in the form of surface density vs. relative pressure, at the surface of I_h ice at 200 K (bottom panel, open symbols) as well as at the surface of LDA ice (full symbols) at 200 K (bottom panel), 100 K (middle panel), and 50 K (top panel), as obtained from our simulations. The insets show these data up to the point where the adsorption layer is still monomolecular (symbols), together with their best Langmuir fits (dashed curves).

Figure 4. Mass density profile of the adsorbed formamide molecules (solid lines) as well as solely of their first molecular layer (circles) in states I (red), II (green), III (blue), and IV (orange), as obtained at the surface of LDA ice at 50 K (top panel), 100 K (second panel), and 200 K (third panel) as well as at the surface of I_h ice at 200 K (bottom panel). The mass density profile of the surface portion of the ice phase is also indicated, for reference (black dashed lines). The inset shows the comparison of the mass density profiles of the I_h (black dashed line) and LDA (red solid line) ice phases along their surface normal axis, *X*, is state I at 200 K.

Figure 5. (a) Definition of the local Cartesian frame fixed to the individual formamide molecules, and of the polar angles ϑ and ϕ describing the orientation of the molecule relative to the ice surface (see the text). (b) Preferred orientations of the formamide molecules at the surface of I_h and LDA ices. (c) Possible H-bonding arrangements of the surface formamide molecules with their formamide neighbors as well as with surface water molecules, when all molecules are aligned in one of their preferred surface orientations. Red, blue, grey, and white balls represent O, N, C, and H atoms, respectively, the dashed lines denote hydrogen bonding, and $\underline{X}$ is the macroscopic surface normal vector, pointing, to our convention, away from the ice phase.

Figure 6. Orientational maps of the first layer formamide molecules, as obtained on LDA ice at 50 K (top row), 100 K (second row), and 200 K (third row) as well as on I_h ice at 200 K (bottom row) in states I (first column), II (second column), III (third column), and IV (fourth column). Lighter shades of grey correspond to higher probabilities. The peaks corresponding to the preferred orientations of the surface formamide molecules (I_{FA} and II_{FA}, see the text) are also marked.

Figure 7. Distribution of the total binding energy (U_b) of the first layer formamide molecules (bottom panels) as well as its contribution coming from the other formamide molecules in the system (middle panels) and from the ice phase (top panels), as obtained (a) at 200 K, (b) at 100 K, and (c) at 50 K at the surface of I_h (full circles) and LDA (solid lines) ices in states I (black), II (red), III (green), and IV (blue). For the definition of the binding energy and its contributions, see the text.

Figure 1

Kiss et al.

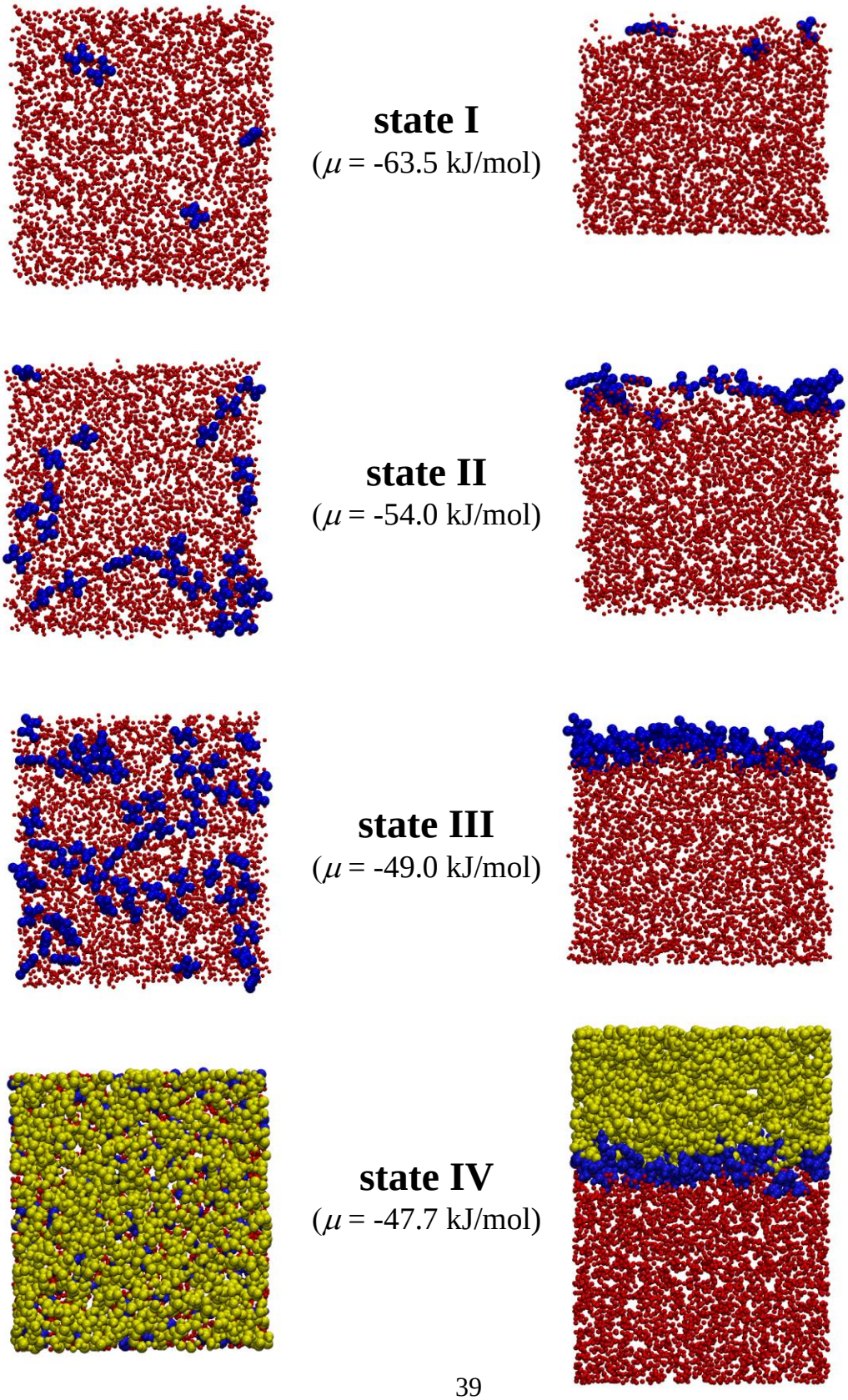

Figure 2

Kiss et al.

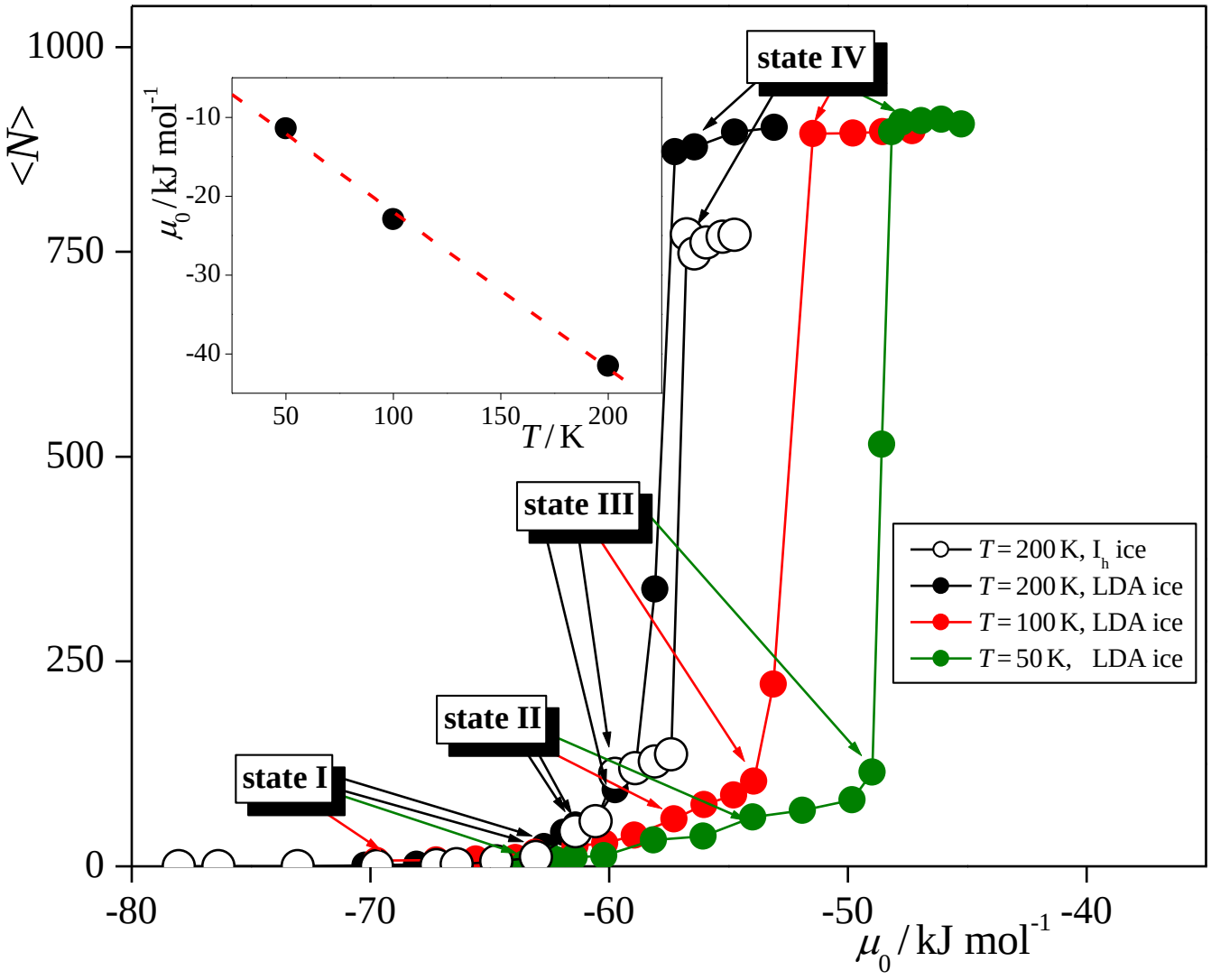

Figure 3

Kiss et al.

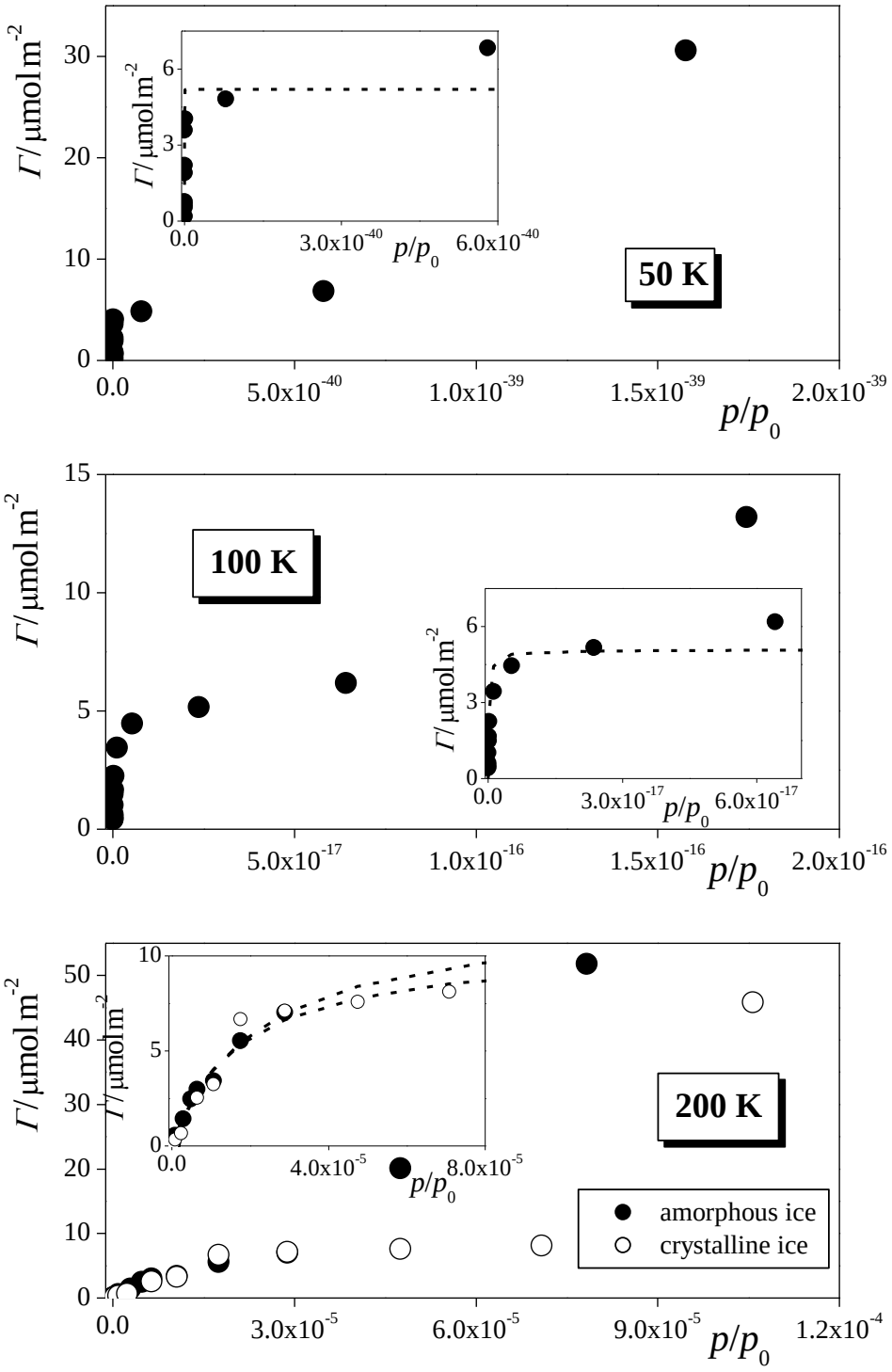

Figure 4

Kiss et al.

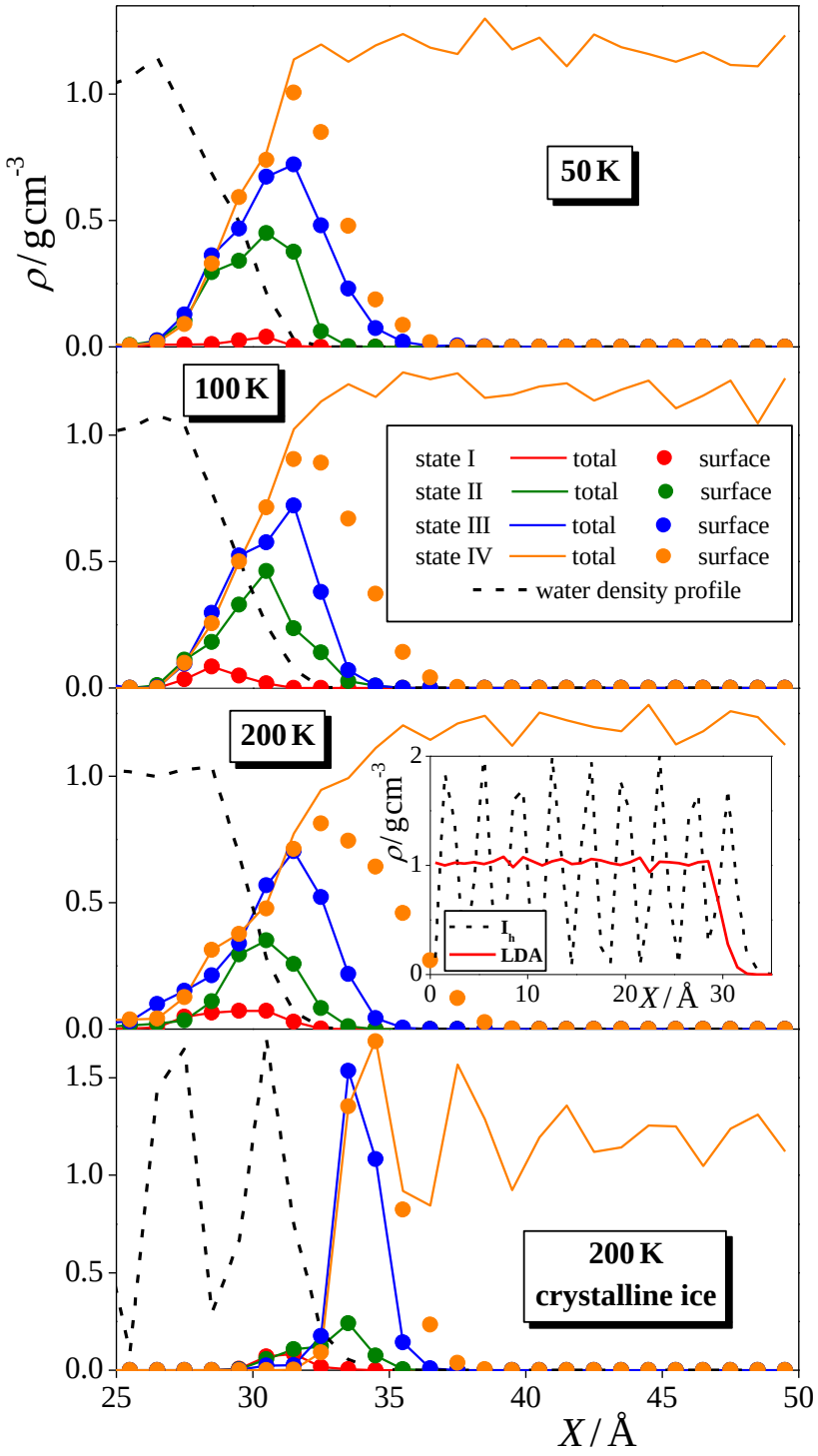

Figure 5

Kiss et al.

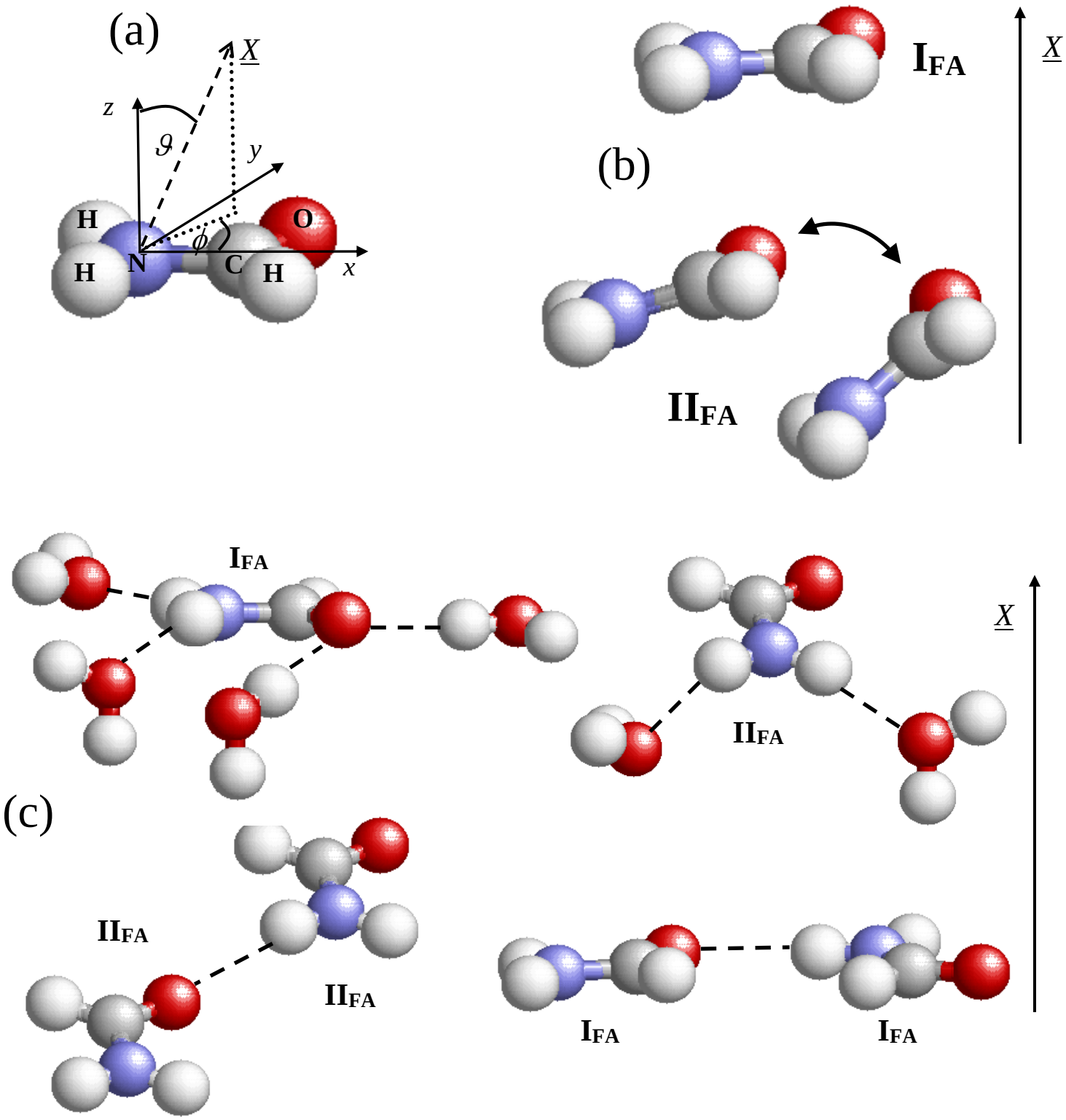

Figure 6

Kiss et al.

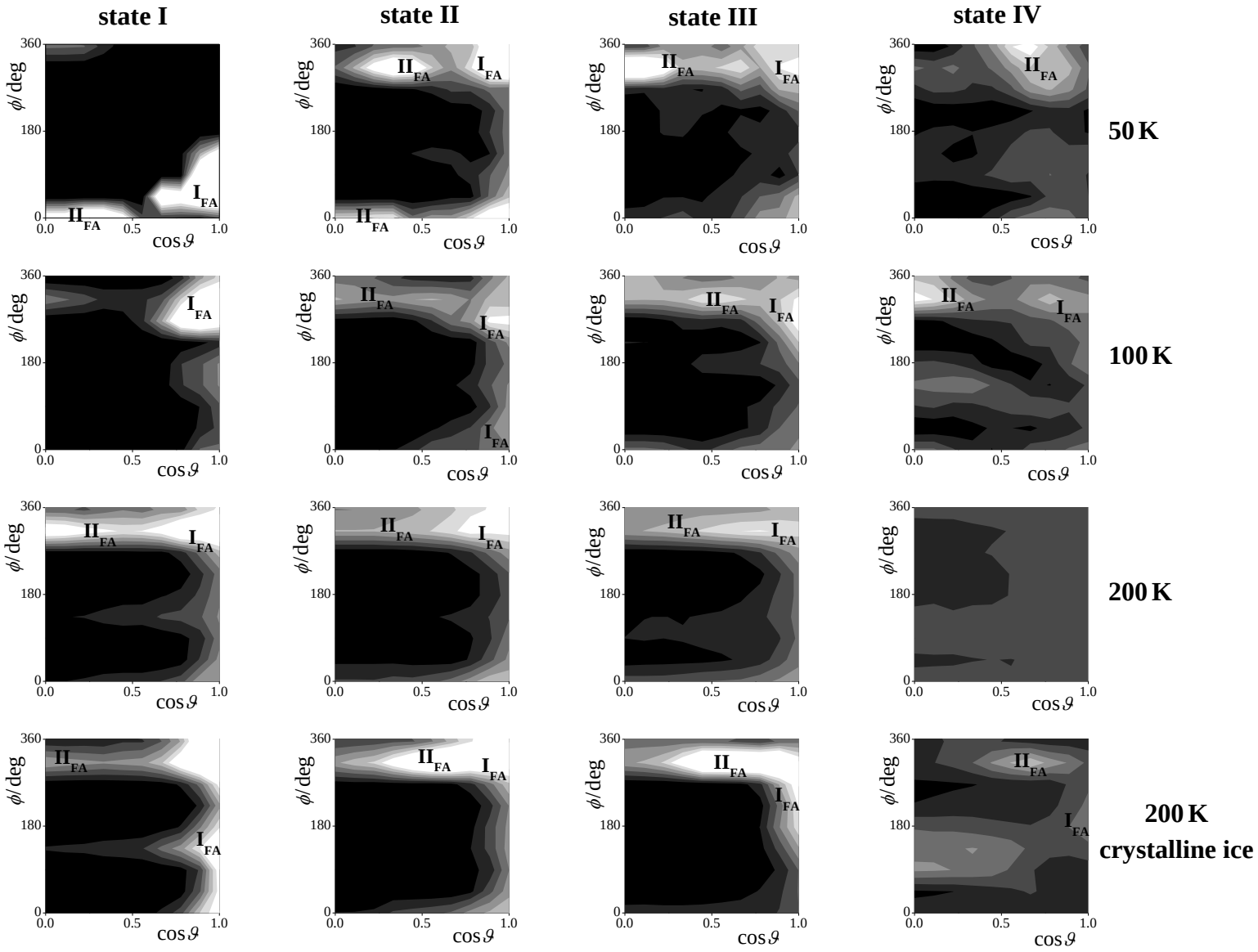

Figure 7a

Kiss et al.

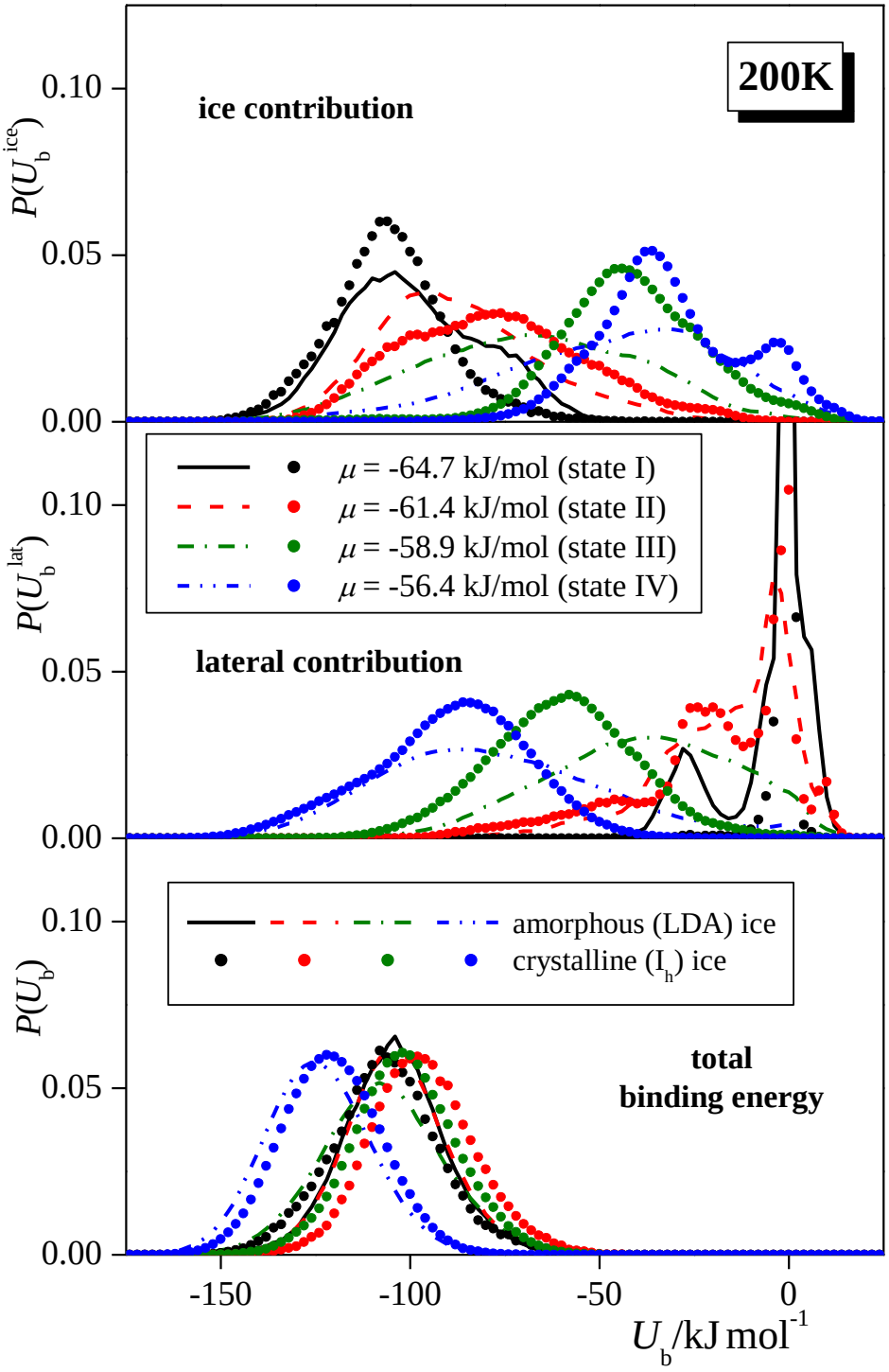

Figure 7b

Kiss et al.

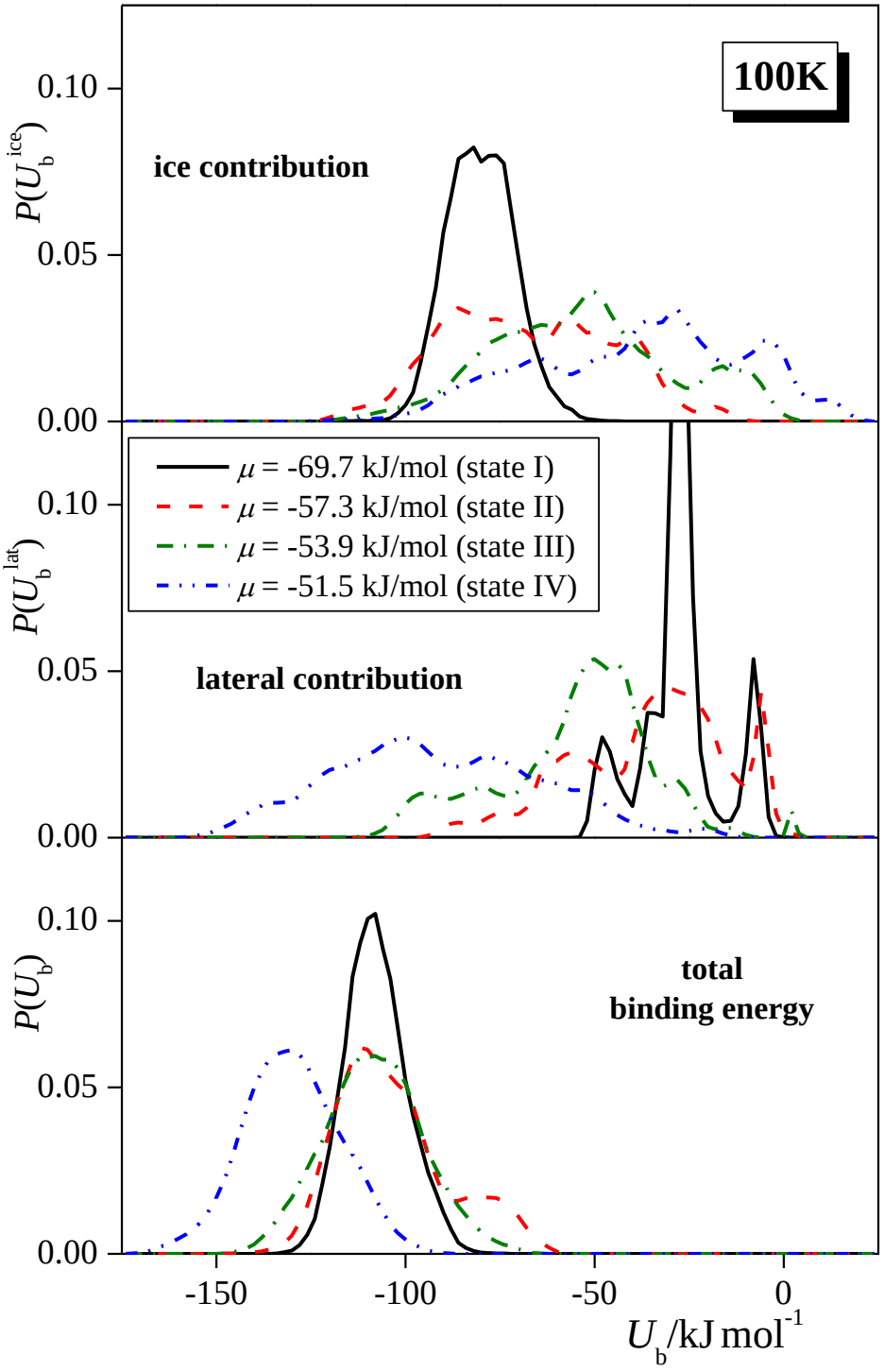

Figure 7c

Kiss et al.

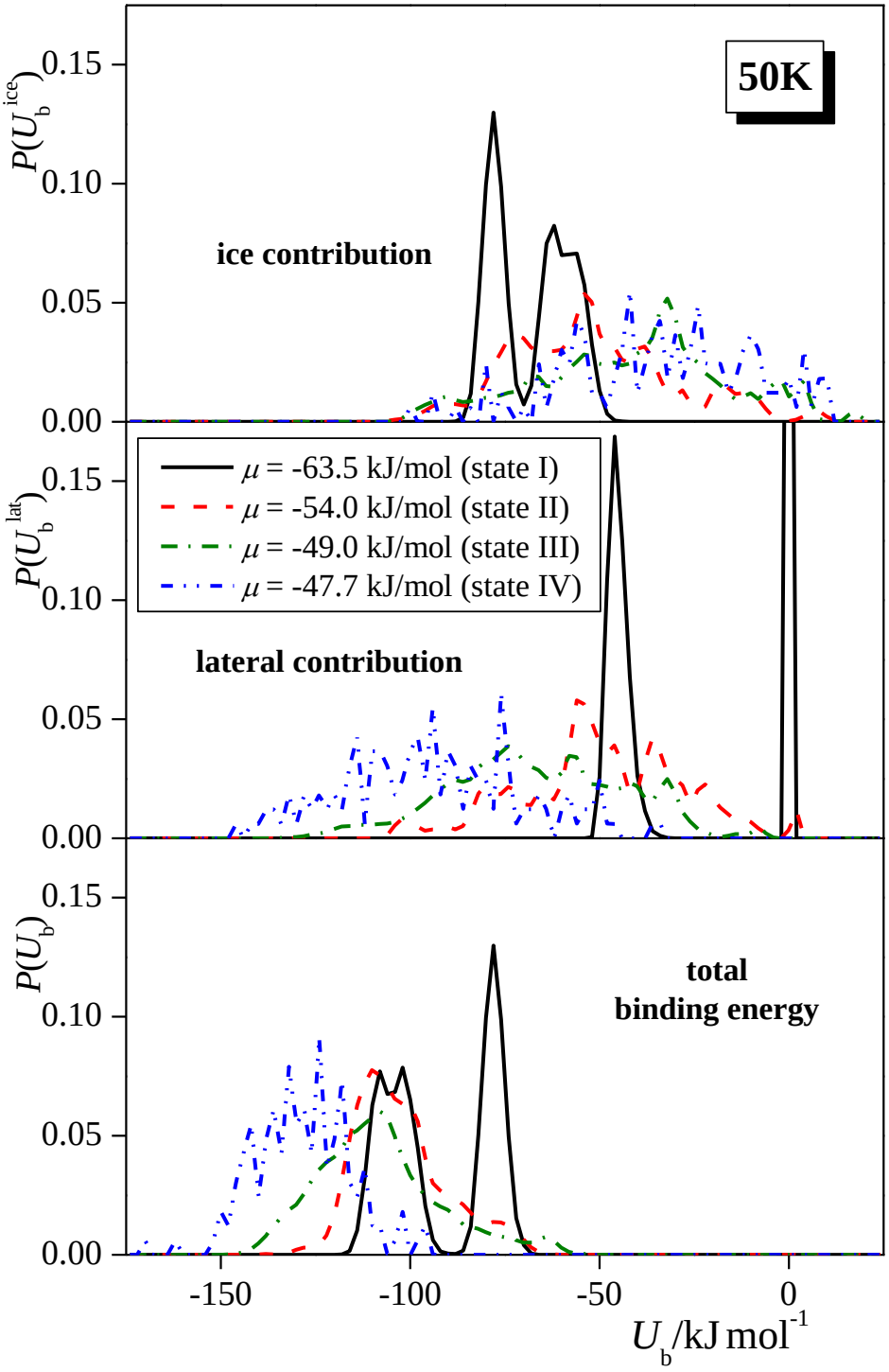

TOC Graphics: